2010-11-11

Mass Transfer and GDL Electric Resistance in PEM Fuel Cells

Lin Wang
University of Miami, lwang@miami.edu

UNIVERSITY OF MIAMI

MASS TRANSFER AND GDL ELECTRIC RESISTANCE IN PEM FUEL CELLS

By

Lin Wang

A DISSERTATION

Submitted to the Faculty
of the University of Miami
in partial fulfillment of the requirements for
the degree of Doctor of Philosophy

Coral Gables, Florida

December 2010

UNIVERSITY OF MIAMI

A dissertation submitted in partial fulfillment of
the requirements for the degree of
Doctor of Philosophy

MASS TRANSFER AND GDL ELECTRIC RESISTANCE IN PEM FUEL CELLS

Lin Wang

Approved:

_____ Hongtan Liu, Ph.D. Professor of Mechanical Engineering	_____ Terri A. Scandura, Ph.D. Dean of the Graduate School
_____ Sadik Kakac, Ph.D. Professor of Mechanical Engineering	_____ Xiangyang Zhou, Ph.D. Assistant Professor of Mechanical Engineering
_____ Angel E. Kaifer, Ph.D. Professor of Chemistry	

WANG, LIN (Ph.D., Mechanical Engineering)

Mass Transfer and GDL Electric Resistance in PEM Fuel Cells (December 2010)

Abstract of a dissertation at the University of Miami.

Dissertation supervised by Professor Hongtan Liu.
No. of pages in text. (91)

Many modeling studies have been carried out to simulate the current distribution across the channel and shoulder direction in a proton exchange membrane (PEM) fuel cell. However the modeling results do not show agreement on the current density distribution. At the same time, no experimental measurement result of current density distribution across the channel and the shoulder direction is available to testify the modeling studies. Hence in this work, an experiment was conducted to separately measure the current densities under the channel and the shoulder in a PEM fuel cell by using the specially designed membrane electrode assemblies. The experimental results show that the current density under the channel is lower than that under the shoulder except when the fuel cell load is high. Afterwards two more experiments were carried out to find out the reason causing the higher current density under the shoulder. The effects of the electric resistance of gas diffusion layer (GDL) in the lateral and through-plane directions on the current density distribution were studied respectively. The experimental results show that it is the through-plane electric resistance that leads to the higher current density under the shoulder.

Moreover, a three-dimensional fuel cell model is developed using FORTRAN. A new method of combining the thin-film model and homogeneous model is utilized to model the catalyst layer. The model is validated by the experimental data. The distribution of current density, oxygen concentration, membrane phase potential, solid phase potential and overpotential in a PEM fuel cell have been studied by the model. The modeling results show that the new modeling method provides better simulations to the actual transport processes and chemical reaction in the catalyst layer of a PEM fuel cell.

ACKNOWLEDGEMENTS

First of all, I would like to sincerely thank Dr. Hongtan Liu, chairman of the dissertation committee, for his professional guidance and constant support during my graduate studies. Whenever I met difficulties in research, not only did Dr. Liu give me invaluable advice, but also encouragement, which molded me to be optimistic and persistent. I will always be grateful for all his help. I also thank Dr. Angel E Kaifer, Dr. Xiangyang Zhou, and Dr. Sadik Kakac for serving in my dissertation committee. I really appreciate the time and effort they devoted, as well as their valuable suggestions to my Ph.D. work. Additionally, I want to thank all the members of the fuel cell lab, especially Tianhong Zhou, Jiabin Ge, Attila Husar, and Andrew Higier, who provided not only valuable help with my research, but also moral support. Moreover, I would like to thank all the professors, staff, and students from the Department of Mechanical Engineering who kindly helped me in one way or another during my Ph.D. program.

Needless to say I am very grateful to my husband, Yikang, my parents, and my elder sister. With their love and moral support, every moment turned out to be sweeter and every step I made turned out to be bigger.

Finally and most importantly, I would like to thank God for His close company, His abundant blessings, and His endless love. God never fails.

TABLE OF CONTENTS

LIST OF FIGURES

LIST OF TABLES

NOMENCLATURE

a	volumetric active surface area, m^2/m^3
C	concentration of a species, mol/m^3
D	diffusion coefficient of a species in a media, m^2/s
E_0	ideal open circuit potential, V
F	Faraday constant, 96,487 C/mol
i	current density produced on the active surface on catalyst particles, (A/m^2)
j_c	transfer current at the cathode side, A/m^3
k_p	hydraulic permeability of the porous layer, m^2
k_h	permeability of the porous layer, m^2
p	pressure, Pa
R	electric resistance, $\Omega \cdot m$
$r^{(2)}$	coefficient in the generalized Darcy's Eq.
S_k	source term of the continuity and species transport equation
T	fuel cell temperature
u, v, w	velocity vector, m/s
x, y, z	coordinates, m

Greek Symbols

α_a	anode transfer coefficient
α_c	cathode transfer coefficient
ρ	density, kg/m^3

ϕ	potential, V
η	totall electrode overpotential, V
σ	ionic conductivity, $\Omega^{-1} \cdot m^{-1}$
ε	porosity
ε_{mc}	volume fraction of membrane in the catalyst layer
μ	viscosity, kg/(m s)

Subscripts

c	cathode
cat	catalyst particle surface
eff	effective
g	gas diffuser
i	inlet
k	k'th component
e	electrolyte phase
s	solid phase
0	surface of the nafion film
xz	the lateral direction in the gas diffusion layer
Y	the through-plane direction in the gas diffusion layer

Superscripts

ref	reference
p	in the pores
nafion	in the nafion film wrapped around catalyst particles

CHAPTER 1

INTRODUCTION

A fuel cell is an energy device which converts the chemical energy of electrochemical reactions into electrical energy directly. Basically a fuel cell is composed of electrolyte and two electrodes. One electrode is called anode and the other is called cathode. When a fuel cell works, fuel is fed to the anode side and oxidant is fed to the cathode side. The electrochemical reactions take place at electrodes. The electrons are produced at the anode side by the reaction and are conducted from the anode to the cathode through the external electric circuit. At the cathode side the electrons are consumed by the reaction. As long as the fuel and oxidant are provided to the fuel cell constantly, the cell will continuously provide electricity. The electrolyte in a fuel cell cannot allow the reactant to go through and cannot conduct electrons, which prevent the fuel and oxidant from mixing directly. Instead, they will participate in the chemical reactions separately at the anode and cathode side. It also assures the electrons to be transported to the external circuit. The fuel cell is characterized by the type of electrolyte and is often named by the electrolyte, such as alkaline fuel cells, the phosphoric acid fuel cells, molten carbonate fuel cells, proton exchange membrane fuel cells etc.

In 1838, Christian Friedrich, a German scientist, discovered the principle of the fuel cell and published it in a scientific magazine. Based on his discovery, the first fuel cell was made by the British scientist Sir William Robert Grove in 1839, which was called “gas battery” (Acres, 2001). In 1955, a chemist from the General Electric Company (GE), W. Thomas Grubb, designed a new type of fuel cell with a sulphonated

polystyrene ion-exchange membrane as the electrolyte. Three years later Leonard Niedrach, another scientist from GE, invented a way of depositing catalyst of platinum onto the membrane, which increased the active reaction area significantly. With this technology improvement, the fuel cell was used for the Project Gemini of NASA. This was the first commercial use of the fuel cell. In 1959, collaborating with his colleagues, Francis Thomas Bacon, a British Engineer, developed a 5KW stationary fuel cell and it was used to power a welding machine. Later Pratt and Whitney licensed Bacon's U.S. patents for use in the U.S. space program to supply electricity and drinking water. After the 1970's, facing the oil crises and environmental pollution, the development of fuel cells has been accelerated driven by the urgent demand of developing new power sources to reduce the dependence on fossil fuels and the amount of exhaust gas. More and more companies and research institutes devoted to fuel cell R&D to realize the mass commercialization of fuel cells. United Technologies Corporation became the first company to commercialize a large, stationary fuel cell system, which can be used in hospitals, universities and large office buildings as a co-generation power plant. Fuel cells are also a candidate of power device for transportation vehicles. Many top automakers are making efforts in hydrogen car R&D, including Honda, Toyota, Nissan, Ford, Hyundai. Honda introduced its first hydrogen car in 1999, which is called FCX. It was followed by its second generation FCX Clarity in 2007. This model is now marketed only in Los Angeles area. Nowadays proton exchange membrane fuel cells are considered the most promising candidate among all types of fuel cells for hydrogen cars.

A proton exchange membrane fuel cell uses a proton exchange membrane as the electrolyte. Among all kinds of fuel cells, the proton exchange membrane fuel cell

(PEMFC) is being commonly considered the best candidate for the vehicular power source to eventually replace the gasoline and diesel internal combustion engines, for its low operating temperature which allows fast startup and transient operation. It can also be applied for portable power, small-scale stationary power and uninterruptible power supplies. R&D efforts through the last decades from private companies and research institutions have pushed PEMFCs to the brink of commercialization.

A representative diagram of a PEMFC is shown in Fig1.1. A typical PEMFC is composed of a solid membrane, two catalyst layers and two gas diffusion layers (GDLs). Those components are pressed together to be one part in real application, called membrane electrode assembly (MEA). Adjacent to the gas diffusion layers, there are two collector plates on which gas channels are grooved. Hydrogen is fed through the gas channel to the anode and it is diffused through the gas diffusion layer to arrive at the catalyst layer, where it is decomposed with the help of the catalyst. The reaction is:

$$2H_2 \rightarrow 4H^+ + 4e^- \tag{1.1}$$

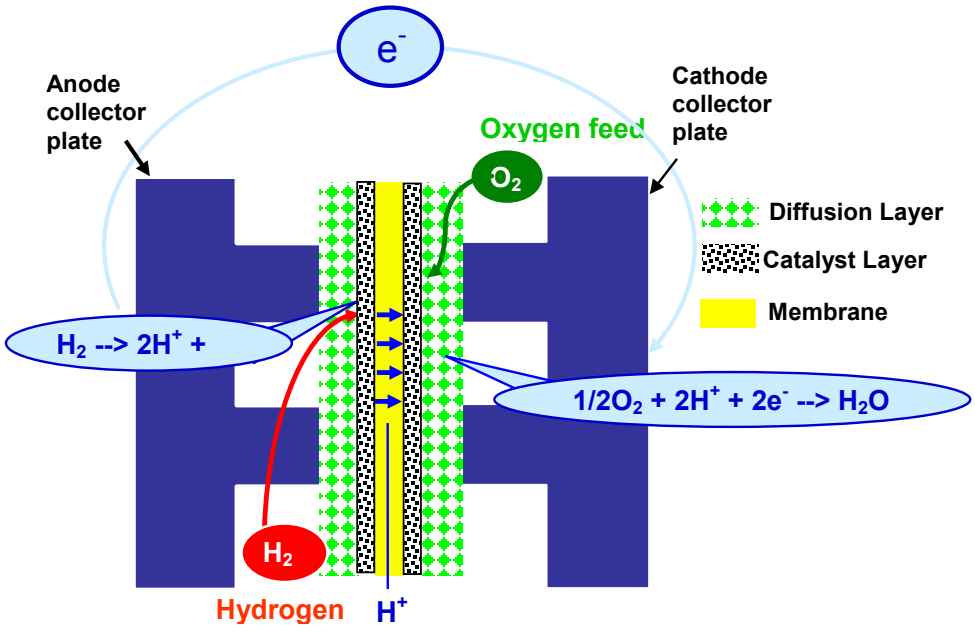

Fig. 1.1 Diagram of a PEMFC.

Protons are conducted through the membrane to the cathode side. The produced electrons are transferred back to the cathode side through the anode diffusion layer, the collector plate and the external circuit. At the cathode side, oxygen is continuously fed through the gas channel. At the cathode catalyst layer the protons combine with the coming electrons and oxygen to produce water and heat:

$$O_2 + 4H^+ + 4e^- \rightarrow 2H_2O \tag{1.2}$$

The common material used for the proton exchange membrane is sulphonated fluoropolymers, usually fluoroethylene. At the beginning, the materials employed by proton exchange membranes were all prone to chemical and mechanical degradation. The poor chemical and mechanical stability remained an issue until mid-1960s when DuPont

invented its ubiquitous Nafion® membrane which has achieved over 50,000 hours of operation. The substantial improvement of the perfluorosulfonic acid proton exchange membrane makes it possible for PEMFCs to meet the needs of widespread terrestrial applications. In 1986, a novel perfluorosulfonic acid membrane developed by the Dow Chemical was used by Ballard and gave four times higher current densities at the same voltage than the standard Nafion® membrane (Prater, 1990). The Dow membrane provides higher water content and proton conductivity at a given temperature compared to the Nafion® membrane. Both Nafion® and Dow membranes exhibit good performance and stability, but their prices are still too high for mass commercialization. Many studies still focus on the development of alternative materials to increase the ion conductivity and reduce the cost.

The function of the electrodes for PEMFCs is to provide the three-phase boundaries for chemical reactions, which have access to the gas reactants, the catalyst particles which accelerate the reactions, and the ionic conductor which supplies the electrons to the reaction site and takes away protons from the reaction site. This process is displayed in Fig. 1.2. To satisfy all these requirements, the fabrication procedure of gas diffusion electrodes is very complicated. Although there are different designs of electrode for PEMFCs, their basic structures are similar. The main component of an electrode is a piece of carbon cloth or carbon paper. They are porous and electron conductive, through which not only the gas reactants can be transferred to the reactant sites and electrons can be transferred from or to the reaction sites. The mixture of catalyst particles, carbon particles and membrane material is impregnated onto the carbon cloth or carbon paper to form the reaction area layer, which is connected to the membrane. The impregnation of

the membrane material into the electrodes allows a dramatic reduction of the platinum loading from 4-8mg/cm^2 to 0.4mg/cm^2 or less while obtaining high power density. The catalyst material used nowadays for PEMFCs is platinum. Another material usually mixed with the catalyst is polytetrafluoroethylene (PTFE), which is hydrophobic to prevent the pores in electrodes from flooding with the water produced by reactions and humidified reactant gases.

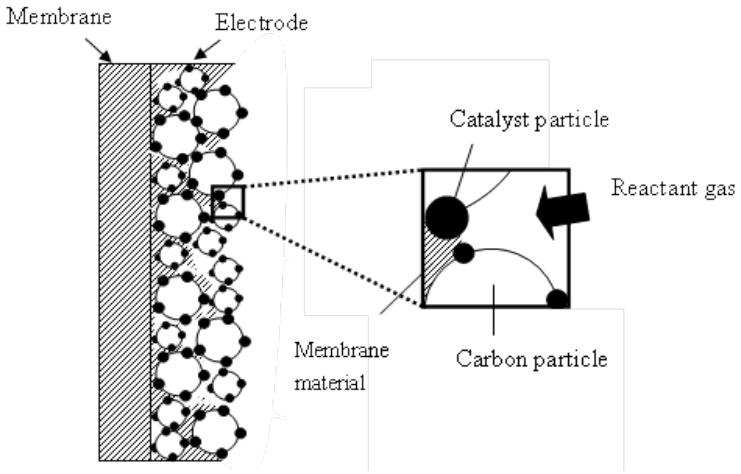

Fig. 1.2 Schematic of the reaction area in a PEMFC.

The collector plate is used to collect and conduct the current, as well as distribute the reactant gases over the surface of the electrodes. An ideal material for the collector plate should have high conductivity, high mechanical solidity, strong resistance to corrosion, impermeability to reactants and low price for automated production. The graphite material is used for the collector plate nowadays because of its high corrosion resistance and low cost compared with the metal materials used before, such as titanium and niobium. The gas channels are machined on the collector plates. There are three main types of channel design: serpentine channel, parallel channel and interdigitated channel. Their schematics are shown below respectively.

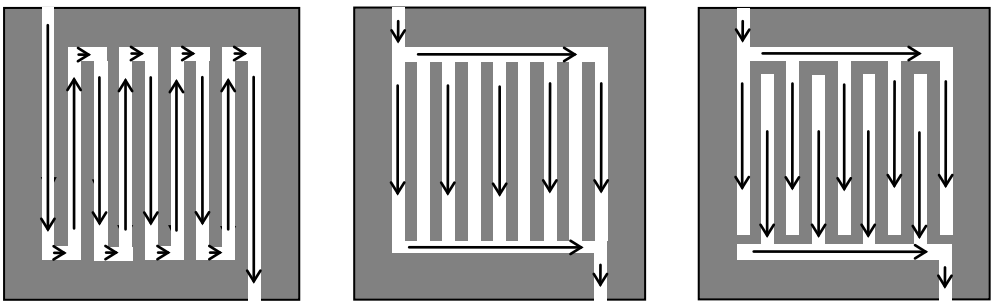

(a) (b) (c)

Fig. 1.3 Flow channels: (a) serpentine (b) parallel (c) interdigitated

Different channel designs will cause different current density distribution, thereby leading to different power output. To improve the channel design, it is necessary to understand how the designs affect the current density distribution. Hence at first this study devises a new method to measure the current density distribution. Secondly a new mathematical model is developed based on the experiment results. This model provides a better simulation to the PEM fuel cell operation.

CHAPTER 2

LITERATURE SURVEY

To improve the performance of PEMFCs, it is important to understand the current distribution inside PEMFCs and how different factors affect the distribution. Different techniques are developed to measure the current distribution in PEMFCs and some valuable data are provided. Yet the available experimental data do not yield a full picture of current distribution inside a PEMFC. Under such circumstances, the numerical modeling plays an important role in simulating and studying the current distribution from more perspectives. These experimental studies on the current distribution and the modeling studies on PEMFCs are reviewed respectively.

2.1 Modeling Studies

2.1.1 Development of modeling studies of PEMFCs

Within the past decade modeling studies on PEMFCs have made fast progress and greatly accelerate the development of PEMFCs. The models of PEMFCs have been developed from one-dimensional to three-dimensional and from single-phase to two-phase. The PEM fuel cells operation phenomena have been simulated extensively.

The performance of the PEMFC largely depends on the performance of the proton exchange membrane. Many modeling studies focus on the transport phenomena within the membrane.

Verbrugge and Hill (1990a) presented a macro-homogeneous mathematical model for the simulation of ion and solvent transport within a

sulfuric-acid/perfluoosulfonic-acid-membrane based on dilute-solution theory. The ion transport through the membrane was described to be driven by the diffusion, migration and convection, which is governed by the Nernst-Planck equation. Solvent transport was driven by pressure and electric-potential gradients. Acid concentration, membrane electric-potential and pressure through the membrane and the pore-fluid velocity as a function of time were obtained by their work. Utilizing this model, the experimental study was carried out to ascertain the ionic diffusion coefficient and membrane pore structure (Verbrugge and Hill, 1990b). Later on, Verbrugge and Hill (1990c) presented the experimental analysis of different perfluorosulfonic acid membranes donated from E. I. du Pont de Nemours and Company, and Dow Chemical Company. The proton, bisulfate ion and water transport characteristics of the membranes were analyzed. The macro-homogeneous model built previously was used to interpret the experimental results. A complete set of analytic solutions was utilized to obtain estimates of the physicochemical parameters from the experimental data. A notable finding was that the Dow polymer yielded more facile proton transport, leading to reduced polarization losses in fuel cell systems, while maintaining lower membrane permeability. It provided a highly desirable quality for water management in fuel cell systems.

Springer et al. (1991) developed an isothermal one-dimensional steady-state model to provide insight into the water transport mechanism in MEA and its effects on fuel cell performance. This was the first time for a model to include water-diffusion coefficients, electro-osmotic drag coefficients, water sorption isotherms, and membrane conductivities as functions of water content based on the experimental data. The water distribution in the model was considered through five regions of unit cross-sectional area:

two inlet channels, two gas-diffusion electrodes and a Nafion® membrane. The diffusion of gases through the porous electrodes was calculated from tabulated data using the Stefan Maxwell equations with a Bruggemann correction that was applied to take account of the electrode porosity. The model assumed water was in the vapor state in the electrodes. Membrane water content at the interface was determined by the activity of water vapor at the electrode/membrane interface.

The modeling results fitted the experimental data well when the measured cell was operated without the presence of the excess liquid water in the cathode. The model predicted a net-water-per-proton flux ratio to be $0.2H_2O/H^+$ under the typical operating conditions, which was as little as one-tenth of the measured electro-osmotic drag coefficient for a fully hydrated membrane. It was also predicted by the model that the membrane resistance increased with the increase of the current density and reducing the thickness of the membrane would alleviate this problem.

Eikerling et al. (1997) developed a random network model to study the micro-porous polymer electrolyte membrane. The model treated the membrane structure as two different types of pores connected by channels in a random way. One type of the pores is water-filled and swollen pore, the other type is dry pore. The model was proposed and investigated by means of an effective medium theory. Specific conductivity and geometrical capacity of membranes were calculated as a function of water content. The conductivity showed a quasi-percolation type dependence.

Many mathematical models include two electrodes and a membrane. All the energy losses in both the electrodes and membrane are involved in the calculation. Such models can predict polarization curves of PEMFCs.

Bernardi and Verbrugge (1991) developed a one-dimensional, isothermal mathematical model which consists of a domain of the cathode gas diffusion layer, an active catalyst layer and a membrane. This was the first time for the model to address the region where part of the membrane phase overlaps with the electrode, which was treated as the active catalyst layer. Their study emphasized on cell polarization characteristics, water transport and catalyst utilization. The membrane model developed by Verbrugge and Hill (1990a) and the gas-phase transport model developed by Bernardi (1990) were employed. In the model, the membrane was fully hydrated and total gas pressure within the gas diffusion layer was constant. Effect of the membrane water content on the ionic conductivity was neglected. The polarization curves were compared well with the experimental results except in the high current density region. The modeling study results indicated that if the membrane maintains full saturation, the membrane resistance becomes significant when the current density is higher than 200mA/cm^2. Reaction rate distribution was calculated in the catalyst layer. It showed that for low current densities the reaction rate distribution is nearly uniform and for high current densities the distribution is highly nonuniform with most of the reaction located at the interface of the diffusion layer and catalyst layer.

Based on the model presented by Springer et al (1991) by which only membrane losses can be evaluated, Springer et al (1993) complemented it to evaluate different types of energy losses at the cathode side in details. The model considered losses caused by: (1) the rate of the oxygen reduction reaction (ORR) process at the Pt/ionomer interface; (2) limited oxygen permeability and limited ionic conductivity within the catalyst layer; (3) limited oxygen permeability through the hydrophobized backing layer; (4) the drop in the

oxygen concentration along the air/O_2 flow channel caused by oxygen reactant consumption. Compared with the modeling work of Bernardi and Verbrugge (1991), which did not consider the effect of the water buildup at the cathode diffusion layer, Springer et al (1993) allowed the liquid water in the cathode to decrease the effective porosity of the diffusion layer. The model was verified by the experimental iR-corrected polarization curves measured. The effects of interfacial kinetics; permeability and conductivity within the catalyst layer and backing-layer parameters such as the effective porosity were studied using the model. The modeling study showed that the gas transport limitation at the cathode diffusion layer determines the cell limiting current density and also affects the slope of the polarization curve in the medium current density domain.

Using a model similar to the Springer et al. (1993), Eikerling and Kornyshev (1998) presented the modeling study focusing on the evaluation of effects of oxygen diffusion, proton conductivity and reaction kinetics in the cathode catalyst layer. It presented catalyst layer analytical results for four different situations: (1) small currents, (2) fast oxygen diffusion, (3) fast proton transport, (4) high current densities. They studied the effect of the catalyst layer thickness, the width, the position of the active fraction of the layer. The dependence of the performance on the oxygen partial pressure was also presented.

You and Liu (2001) also presented a parametric study of the cathode catalyst layer using a pseudo-homogeneous model. The one-dimensional model has following assumptions: (1) The carbon matrix has good electron conductivity, thus the potential drop among solid matrix can be neglected compared with the potential drop in the electrolyte phase; (2) The catalyst Pt particle is uniformly distributed; (3) the water

content within the ionomer is constant; (4) the oxygen diffusion coefficient is constant. The model was developed by control volume method and was solved using relaxation method. The effect of the overpotential, proton conductivity, porosity of the diffusion layer and catalyst surface area were studied. In their work, it was concluded that the best solution for optimization of the cathode catalyst layer performance is to minimize the thickness of the catalyst layer while optimizing the combinations of the parameters.

Another one-dimensional, isothermal mathematical model for the Ballard Mark IV proton exchange membrane fuel cell was developed by Amphlett et al. (1995). Considering the mechanical approach could not adequately model fuel cell performances, since several simplifying approximations were used in order to facilitate model development; a combination of mechanistic and empirical modeling techniques was employed. Mass transport properties were considered by using Stefan-Maxwell equations. Thermodynamic equilibrium potentials were defined by the Nernst equation. Activation overpotential was defined through a Tafel equation. By comparing the modeling results with the experimental data, two empirical equations of activation overpotential and the internal electrical resistance of the cell were obtained. The modeling results by using these empirical equations compared well with the experimental data.

Gurau et al. (2000) developed a one-dimensional half-cell model for the PEMFC. The model included a gas channel, a gas diffusion layer, a catalyst layer and a membrane at the cathode side. The purpose of the work was to derive analytical solutions for a mathematical model that was coupled with the phenomena in the cathode gas channel, gas diffusion layer, catalyst layer and membrane. The presence of liquid water in the gas diffusion layer and catalyst layer was taken into account by means of effective porosities.

To account for liquid water concentration gradient and composite structure that characterize the gas diffusion layers, the gas diffusion layer in the model was represented by a series of parallel layers defined by different porosity-tortuosity coefficients. Based on the oxygen mass transport equation and Ohm's law for proton migration, the expressions for the oxygen mass fraction distribution in the gas channel, gas diffusion layer and catalyst layer; current density and membrane phase potential in the catalyst layer and membrane were derived.

The two-dimensional models provide tools for people to get more understanding of PEMFCs. Fuller and Newman (1993) established a pseudo two-dimensional mathematical model using the centered solution theory for the PEMFCs. The geometrical model includes two gas diffusion layers, two reaction zones and a membrane. Although they considered the modeling domain in two dimensions, they solved for the transport only in y direction at a given value of z and integrated down the membrane-electrode assembly in the z direction (y direction is the direction perpendicular to the MEA surface, z direction is along the height of the MEA). Heat and water management and the utilization of fuel were studied in details. They showed that the rate of heat removal is a critical parameter in the fuel cell operation.

Nguyen and White (1993) also developed a pseudo two-dimensional mathematical model to investigate the effectiveness of various humidification designs. The model region consists of two flow channels on both sides of the membrane. The electrode layer was assumed "ultrathin" and the gas diffusion through the electrode porous layer was neglected. The influence of liquid water content on ionic conductivity and the enthalpy change due to phase change was taken into account. The modeling

results showed that the back diffusion of water from the cathode to the anode is insufficient to keep the membrane hydrated when power density and energy efficiency are high. Therefore, gases at anode side must be humidified. It was shown that if air is used at the cathode side, it should be humidified.

All the models discussed above concerned the transport phenomena in the domains consisting of a membrane, catalyst layers, and gas diffusion layers without combining the simulation of physical process in gas channels, so that the concentration and partial pressure in gas channels were assumed in an arbitrary way. Usually average values were used as boundary conditions at the interface. Fuller and Newman (1993) assumed the gas outside the gas diffusion layers to be uniform composition in the direction across the cell. Nguyen and White (1993) employed the algebraic expressions for the concentrations along the electrodes. Amphlett et al. (1995) assumed the average partial pressure along the gas channels. However, the concentration along the gas channel, gas diffusion layers and catalyst layers will be varied due to the diffusion-convection transport and electro-kinetics in the catalyst layers in different locations. Therefore, these distributions will depend on the gas/medium properties, as well as on the reaction rates. These properties and reaction rates are in turn functions of the reactant concentrations so that an iterative procedure would be required to predict them. Moreover they ignored the convection mechanism for the mass transport through the porous media. Later on, some comprehensive models were developed to complete these aspects.

Gurau et al. (1998) was the first to develop a two-dimensional comprehensive mathematical model involving the momentum equations in the coupled gas channel-gas

diffusion layer-catalyst layer domain, so that the interaction between the gas channels and the rest parts of a fuel cell was described without any assumption. The geometrical domain includes two gas channels, two gas diffusion layers, two catalyst layers and a membrane. In each layer of the domain, the physical process was governed by the continuity equation, momentum equation, energy equation and mass transport equation. In the model, three different domains were considered with respect to the phases of the fluid: the gas channel, gas diffusion layer and catalyst layer at the cathode side for the air mixture; the gas diffusion layers and catalyst layers at both the anode and cathode sides and the membrane for liquid water; the gas channel, gas diffusion layer and catalyst layer at the anode side for hydrogen. Each domain was considered as an entirety so that no boundary condition was needed at the interface between layers in the domain. They found non-linear oxygen mole fraction distribution along the flow channel direction, which is different from pervious assumption of linear distribution in pseudo two-dimensional models (Nguyen and White, 1993). They also obtained the oxygen and water concentrations in the gas channel and gas diffusion layer and studied the influences of some parameters on the cell performance including porosity, temperature, and fluid velocity.

Yi and Nguyen (1998) also presented a two-dimensional steady state mathematical model. The effect of different heat exchangers on current distribution along the channels was studied. The results showed that the current distribution along the channel with the counter-flow heat exchanger was most uniform among all and had better performance. Um et al. (2000) developed a transient two-dimensional model to study the hydrogen dilution effect and the transient response of current density to the change of the

cell voltage. To better simulate the phenomena with the existence of liquid water inside PEMFCs, the two-phase models were developed by Wang et al. (2001), and You and Liu (2002). Polarization curves, water and oxygen concentration distributions within both single- and two-phase regimes of the air cathode were reported. The models discussed above all consider the directions along the channel and that through the different layers of PEMFCs.

Other two dimensional models consider the directions across the channel and the shoulder, and through the different layers of a PEMFC. Natarajan and Nguyen (2001) developed a two-dimensional and two-phase model, which does not consider the electron transport. The modeling results showed the current distribution across the direction of the channel and the shoulder with different thickness of diffusion layer, different channel and shoulder sizes and different channel-to-shoulder ratios. In all these cases the current density under the shoulder was always lower than that under the channel because of the lower reactant concentration under the shoulder. Later Lin and Nguyen (2006) developed a two-dimensional, two phase model based on the one-dimensional model presented in Lin et al. (2004). The electron transport phenomenon was considered in this model. The current distribution across the channel and the shoulder direction was simulated with different in-plane electronic conductivities of the gas diffusion layer. The result showed that when the in-plane electronic conductivity was as low as 2s/m, the current density under the shoulder is higher than that under the channel; however the cell performance had small change with different in-plane electronic conductivities.

Not satisfying with the previous modeling studies, researchers continued to develop three-dimensional PEM fuel cell models. Dutta et al. (2000) first published a

three-dimensional CFD model developed by Fluent^{TM}, a commercial CFD software. The current density distribution along the channel under with different membrane thickness and cell voltage were simulated. Zhou and Liu (2001) developed a three-dimensional CFD model from scratch. Comprehensive modeling results were reported on reactant velocity, oxygen concentration, water concentration, temperature distribution and current distribution. The current distribution across the channel and shoulder direction was reported and showed that the current density under the shoulder was always lower than that under the channel caused by the lower oxygen concentration under the shoulder. Zhou and Liu (2006) added the electron and proton transport phenomena to the previous model to study the current distribution across the channel and the shoulder direction. The modeling results showed a different current distribution under the channel and the shoulder from the previous modeling results when the electronic conductivity of the diffusion layer became low. However the current density under shoulder was still lower than that under the channel with any electronic conductivity. Um and Wang (2003) presented a three-dimensional model to study the performance of PEMFCs with interdigitated flow field. Ju and Wang (2004) also presented a modeling study on current distribution along the gas channel. The modeling results were validated by experimental data and the comparison showed good agreement. Meng and Wang (2004) developed a three-dimensional model to investigate the effect of electron transport on PEMFCs, which is the first model considering the electron transport inside PEMFCs. The modeling results showed that the current density under the shoulder became higher than that under the channel when the electronic conductivity of gas diffusion layer was as low as 30s/m.

In this model the in-plane electronic conductivity and the through-plane electronic conductivity were not differentiated.

The research group led by Djilali carried out a series of modeling studies on PEMFCs as well. Berning et al. (2002) published a three-dimensional non-isothermal model, in which the electron transport was not included. The modeling results showed that the oxygen concentration determined the current distribution, and the current density under the shoulder is always lower than that under the channel. Later two new three-dimensional models using Fluent^{TM} and CFX^{TM} were developed and electron transport was coupled into the model by this group. The new modeling results of current distribution reported in Nguyen et al. (2004) and Sivertsen et al. (2005) showed that when the electronic resistance of the gas diffusion layer was as low as 100s/m, the current density under the shoulder was higher than that under the shoulder at low load operation.

Shimpalee et al. (2004) presented a three-dimensional model to study on current distribution on MEA in a commercial-size PEMFC with multiple serpentine channels. The results showed that the current decreased along the channel from the inlet towards the outlet. The current distribution with dry cathode feed and humidified cathode feed were compared and the current distribution with the dry cathode feed were more uniform but the performance was worse. The results didn't show a detailed comparison of the current under the shoulder and under the channel.

Birgersson and Vynnycky (2006) developed an isothermal three-dimensional model. The current distributions across the channel and the shoulder with different types of flow field were calculated, which showed the current density under the shoulders was

lower than that under the channels with the parallel flow field. In this model the electron transport in fuel cells was not considered.

2.1.2 Development of methods modeling the catalyst layer of a PEMFC

Catalyst layer is the most important and complicated component in a PEM fuel cell. It is where the chemical reaction happens. At the cathode side of a PEM fuel cell, in the catalyst layer there must be access to get oxygen from the diffusion layer, protons from the membrane, as well as electrons from the anode. Consequently the catalyst layer is a porous media composed by mixing carbon particles, catalyst particles, electrolyte material and hydrophobic material of PTFE. Different methods have been developed to model the catalyst layer of a PEMFC in the mathematical models. Generally the catalyst models can be categorized into four groups: ultra-thin layer model, pseudo-homogeneous model, agglomerate model and thin-film agglomerate model.

In the ultra-thin layer models, the catalyst layer is treated as an interface between the diffusion layer and the membrane. Only the chemical reaction in the catalyst layer is considered, which is governed by the Tafel or Butler-Volmer equation. Springer et al. (1991), Natarajan and Nguyen (2001), Wang et al. (2001) and Berning et al. (2002) employed this method in their models.

The second group of the models treats the catalyst layer as a homogeneous medium. The mass transport of reactant through the pores from the gas diffusion layer to the active surface on catalyst particles is considered and governed by the molecule diffusion mechanism. Bernardi and Verbrugge (1991, 1993), Um et al. (2000, 2003), Ju and Wang (2004) modeled the catalyst layer as a homogeneous medium with continuous distribution pores filled with Nafion material. The oxygen from the diffusion layer first

dissolved in the Nafion medium and then diffused to the catalyst particle surface. Other models treated the catalyst layer as a homogeneous medium with continuous distribution of dry pores in the catalyst layer, including Springer et al. (1993), Fuller and Newman (1993), Nguyen and White (1993), Eikerling and Kornyshev (1998), Gurau et al. (1998, 2000), Zhou and Liu (2001, 2006), Meng and Wang (2004), Nguyen et al. (2004), Sivertsen and Djilali (2005).

The agglomerate model of the catalyst layer of a PEM fuel cell is developed based on the "flooded agglomerate" model reported by Giner and Huner (1969). They first proposed a model of the Teflon-bonded electrode based on its structure with double-scale porosity. The electrode is made up a number of porous cylinder agglomerates, which are flooded with electrolyte. Between the agglomerates, there are hydrophobic gas pores coated with Teflon. Under the operation, the reactant gas diffuses through the gas pores between the agglomerates, and then dissolves into the electrolyte contained in the agglomerates and diffuses through the electrolyte until it participates in the chemical reaction on the active surface on catalyst particles. Later different geometries of agglomerates were used in the models of PEM fuel cells, including slab, cylinder and sphere. These models include, Gloaguen and Durand (1997) and Wang and Song et al. (2004).

Gloaguen and Durand (1997) presented a comparison of a pseudo-homogeneous model and an agglomerate model. The slab geometry of agglomerate is considered. They concluded that the agglomerate model is more appropriate to simulate the catalyst layer than the pseudo-homogeneous model. The modeling results showed that the pseudo-homogeneous model overestimates the limitation of oxygen transport.

Wang and Song et al. (2004) presented a spherical flooded-agglomerate model for the cathode catalyst layer. The oxygen transport in the pores, dissolved oxygen diffusion through electrolyte and the oxygen reduction on the catalyst active surface are included in the model. The effects of the porosity, agglomerate size, catalyst layer thickness and proton conductivity on the performance of a PEM fuel cell were studied.

Will (1963A) first presented a thin film model to deal with the diffusion and ohmic control of an electrode. In this model, a thin film electrolyte was wrapped around the electrode. The reactant gas has to dissolve and diffuse through the film to arrive the electrode interface and participate in the chemical reaction. This transport process was observed by Will's experiment (Will, 1963B).

Later the reactant transport process through the thin film of electrolyte has been incorporated into many mathematical models of PEM fuel cells. Some agglomerate models also coupled this transport process. These models are Broka and Ekdunge (1997), Siegel et al. (2003), Lin et al. (2004), Wang et al. (2004), Jaouen et al. (2002), Lin and Nguyen (2006), and Madhusudana and Rengaswamy (2006).

Broka and Ekdunge (1997) used a thin-film agglomerate model to simulate the PEM fuel cell cathode. The polarization curves have been simulated with different values of oxygen permeability, effective conductivity and thickness of the active catalyst layer, as well as thickness of the Nafion$^{@}$ film wrapping the agglomerates. The polarization curves obtained by the thin-film agglomerate model are compared with experimental results and the curves simulated by a pseudo-homogeneous model. It is presented that the thin-film agglomerate model provides better simulation to the experimental polarization curves than the pseudo-homogeneous model.

Siegel et al. (2003) developed a two-dimensional steady state mathematical model, which used the agglomerate model for the catalyst layer. This model calculates species transport, electrochemical kinetics, energy transport, current distribution, and water transport in the catalyst layer. The performance of a PEM fuel cell is studied with different volume fractions of gas pores and polymer membrane contained within the catalyst layer, as well as the geometry of the agglomerates.

Lin et al. (2004) developed a two-phase, one-dimensional steady state model of membrane electrode assembly of a PEM fuel cell. The catalyst layer is described to be composed by many agglomerates of cylindrical pellet geometry wrapped by a thin film of Nafion. The model was used to study the effect of water flooding in the gas diffusion layer and catalyst layer of the cathode on the cell performance. It was found that the flooding problem in the catalyst layer is more severe than that in the gas diffusion layer.

Wang et al. (2004) studied the characteristic of catalyst layer using two thin-film agglomerate models. In one model, the pores of an agglomerate are fully filled with proton conducting perfluorosulfonated ionomer. In the other model, the pores of an agglomerate are fully filled with water. The first model is rationalized on the basis of the Thiele-modulus. The latter model is studied using Nernst-Planck and Poisson equations. Current production, reactant and current distribution and catalyst utilization are studied by the models. In addition, an analytical solution was obtained for a planar geometry of agglomerates.

Jaouen et al. (2002) developed a one-dimensional steady-state fuel cell model using a thin film spherical agglomerate model for the catalyst layer. The modeling results were compared with experimental data. The modeling result showed a doubling of the

Tafel slope at the high current densities caused by the limitation of proton migration in the active layer or by oxygen diffusion in the agglomerates. The dependence of the reaction rate on the active-layer thickness, oxygen pressure, and relative humidity of the gas were simulated by the model. Moreover, a mathematical expression for the limiting current density due to the slow gas phase diffusion, which can be used to correct the polarization curves for slow gas phase diffusion.

In the two-dimensional two-phase model presented in Lin and Nguyen (2006), the thin film agglomerate model was applied to the catalyst layer. In this model, oxygen has to dissolve into the water film which is in the pores, and then diffuse through the water film and Nafion film to reach the surface of the catalyst pellets.

Madhusudana and Tengaswamy (2006) presented a dynamic model for spherical agglomerate in a PEM fuel cell. The model was used to study transient response of the agglomerate potential and concentration of dissolved oxygen, as well as agglomerate current to step changes in surface boundary conditions. The results showed that the time scales for the agglomerate potential and concentration of dissolved oxygen to respond are different by several orders of magnitude.

Very few modeling work has coupled the thin film model with the pseudo-homogeneous model for the catalyst layer. Marr and Li (1999) considered the diffusion of dissolved oxygen through the Nafion film before arriving at the active surface in their pseudo-homogeneous model of the catalyst layer. However, they did not model the real diffusion process; instead, they simulat this process by decreasing the effective diffusivity of reactant in the catalyst layer.

2.2 Experimental Studies on Current Distribution

During the last decade, many experimental studies have been carried out to measure and study the current distribution. Various techniques have been developed to measure the current distribution. Most of these techniques enable the measurement of current density either along the channel or in large segments. Very few experimental data of the current density variance in the catalyst layer across the channel and the shoulder direction are available.

2.2.1 Current distribution along the channel

Brett et al. (2001) measures the current distribution dynamically along a single channel using the printed circuit board approach. The current distribution is studied under different polarizations and air flow rates. The study shows the depletion of reactant along the channel and slow reaction rate at low air flow rate.

Mench et al. (2003) also presented an experimental study on current distribution measurement along a serpentine channel. They used a segmented flow field with current-conducting wires. The effect of cathode flow rate on the current along the channel was studied and mass-limited performance was observed. The transient current density was measured, which showed a slow flooding process until the steady state was arrived.

The research group of Nguyen has carried out a series of experimental studies on current distribution. Firstly a study of measurement of current density and potential distribution along a straight channel was developed and reported in Natarajan and Nguyen (2004). The segmented current collector and flow field was used. The current distribution with both the segmented and the unsegmented electrodes of two commercially available gas diffusion layers from SGL-CARBON Inc. and ETEK Inc.

were measured. Based on this experimental work, further experiments studying the effects of reactant flow rates, gas stream humidity and cell temperature on the PEM fuel cell were carried out. The experimental results were presented in Natarajan and Nguyen (2005(1), 2005(2)). The flooding problem is observed to be more serious under lower oxygen flow rates and higher anode temperature. In addition, the significant deterioration of performance caused by dry fuel is presented. It is presented that the current distribution is affected by reactant flow rates, gas humidity and cell temperature at the same time, therefore the performance of a fuel cell is determined by the integrated effect of all these factors.

2.2.2 Current distribution in large segments

Cleghorn et al. (1998) presented the method of printed circuit board approach of measuring current distribution for the first time. The current collector, flow field and electrode were composed of large segments. The current collected on each segment was measured. The current distribution was studied under different stoichiometric flow of air. Under the high stochiometric ratio of air, the increase of the current from the inlet to the outlet was observed, which was explained by the increase of the membrane conductivity along the gas flow direction. However under the low stoichiometric ratio, the air concentration became a dominant factor causing the degradation of the local performance from the inlet to the outlet.

Three in-situ methods of measuring current distribution in PEM fuel cells were presented in Stumper et al. (1998). One of them is partial MEA approach. The local current produced at a part of the catalyst layer was measured by using MEA with partially loaded catalyst. The second method is subcell approach; in which a few isolated

subcells were placed in the MEA and current were collected from the subcells respectively. This method has been used by Rajalakshmi et al. (2002) and Liu et al. (2005) to measure the current distribution. The third method is the current mapping technique, which employs a passive resistor network distributed over the whole MEA area. Later Ghosh et al. (2006) measured the current distribution of a fuel cell under different operation conditions using the same method. The difference between their works is that Ghosh et al. used a segmented expanded graphite plate as a passive resistor network, while Stumper et al. used a graphite element between the bipolar plate and end plate. The advantages and disadvantages of these three methods were compared.

Wieser et al. (2000) presented a new technique of using magnetic loop array to measure the current distribution. The flow field of straight channels was segmented and attached with annular ferrites and hall sensors. Some sample current distribution data was displayed in the paper.

Several studies on measurement of current distribution have been carried out in the Laboratory of Advanced Energy Systems of Helsinki University of Technology of Finland. Noponen et al. (2002) developed a PEM fuel cell with segmented collector plate to measure the current distribution in a free-breathing PEMFC and studied the effect of the cell temperature on the current distribution. Afterwards, the study of the effect of varying ambient conditions on the current distribution using the method was presented in Hottinen et al. (2003). Further study (Noponen et al. (2004)) on the effects of inlet humidification, gas composition at the cathode side and the flow geometry on the current density were carried out. Both segmented and unsegmented gas diffusion layer were used.

Hakenjos et al. (2004) presented an experimental study on current distribution measurement using a segmented flow field with straight channels. With the same experimental setup, they carried out another study to measure the local electrical impedance spectra simultaneously with the measurement of current distribution (Hankenjos and Hebling (2005)). In the mean while, this research group also set up another test fuel cell with segmented anode flow field and partially segmented gas diffusion layer, with which the current, temperature and water distribution were measured under operation simultaneously. Later using the same experimental setup the current, impedance, heat and water distribution of two types of flow fields were measured and compared, which was presented in Hogarth et al. (2006).

Büchi et al. (2005) developed a PEM fuel cell with semi-segmented collector plate to study the effect of water management on current distribution. The semi-segmented plate has a regular flow field on one side and segmented electricity collector on the other side.

Sun et al. (2006) presented a new technique of measurement of current distribution. In the test fuel cell, a measuring gasket with a few strips was inserted between the flow field plate and the gas diffusion layer. The current produced in the part of the catalyst layer corresponding to each strip is measured. The effects of gas humidification, cell temperature, reactant flow rate and pressure on current distribution were studied.

2.2.3 Current distribution across the channel and the shoulder direction

Freunberger et al. (2006) presented an experimental study on current distribution across the channel and the shoulder direction of a PEM fuel cell for the first time. A

special experimental setup was designed and local potential was measured. The current density was not measured directly, but calculated from the ohmic drop in the electron conductors of the cell. The experimental results showed that at the low load, the current density under the shoulder is higher than that under the channel; at the high load, the current density under the channel is higher. This is the only experimental study on current distribution across the channel direction.

2.3 Objectives

Understanding current distribution in a PEMFC and the factors affecting the distribution is important for optimizing the design of a PEMFC. Therefore studies have been carried out extensively. Among these studies, one branch is to study the current density distribution in the catalyst layer across the gas channel and the collector plate shoulder direction, shown as the z direction in Fig. 2.1. Two gas channels and one shoulder are shown in Fig. 2.1. Oxygen is fed along the gas channels and diffuses through the gas diffusion layer and catalyst layer. Electrons are conducted through the external circuit from the anode side of the fuel cell to the cathode collector plate. Conducted through the shoulder, electrons will arrive at the gas diffusion layer and be conducted throughout the gas diffusion layer and the catalyst layer.

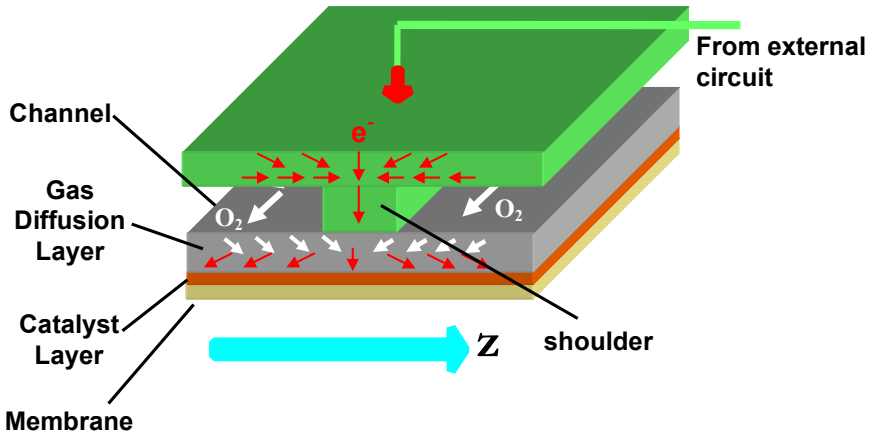

Fig. 2.1 Schematic of the mass and electron transport at the cathode side of a PEM fuel cell.

The Butler-Volmer equation, equation (2.1), which governs the current production in a PEM fuel cell, shows that the current density is affected by both the oxygen concentration and the overpotential.

$$j_c = (ai_0^{ref})_c \frac{c_{O_2}}{c_{O_2}^{ref}} (e^{\frac{\alpha_c^a F}{RT}\eta_c} - e^{-\frac{\alpha_c^c F}{RT}\eta_c}) \tag{2.1}$$

Two factors affect the overpotential: one is the lateral electric conductivity in the gas diffusion layer; the other is the through-plane electric conductivity of the gas diffusion layer (The lateral direction and the through-plane direction are shown in Fig. 2.2). Therefore different electric conductivity distribution will lead to different current density distribution.

The current density across the gas channel and the gas collector shoulder has been widely studied by many mathematical models. Different assumptions of the electric conductivity are used and led to different simulation results of current density distributions.

The models developed at the early stage are all based on the assumption that the electric conductivities of the collector plate, gas diffusion layer and catalyst layer are infinity. In other words, the overpotential distribution is uniform in a PEM fuel cell. Some of these models [Natarajan and Nguyen (2001), Zhou and Liu (2001), Berning et al. (2002), Birgersson and Vynnycky (2006)] simulated the current density distribution across the channel and the shoulder direction. The modeling results showed that the current density under the shoulder is lower than that under the channel, since oxygen concentration is a dominant factor deciding the current density distribution. Natarajan and Nguyen (2001) presented that the current density under the shoulder is significantly lower than that under the channel and it is even close to zero.

Later, some models of a PEM fuel cell [Lin and Nguyen (2006), Zhou and Liu (2006), Meng and Wang (2004), Nguyen et al. (2004), Sivertsen et al. (2005)] started to consider the finite electric conductivities of the collector plate, gas diffusion layer and the catalyst layer. Moreover in the gas diffusion layer the electric conductivities in both the lateral direction and the through-plane direction were considered. Due to the finite electric conductivity, overpotential distributions in the catalyst layer in these models are not constant anymore, which is shown in Fig. 2.2. Consequently different current density distributions across the channel and the shoulder direction are obtained by these models.

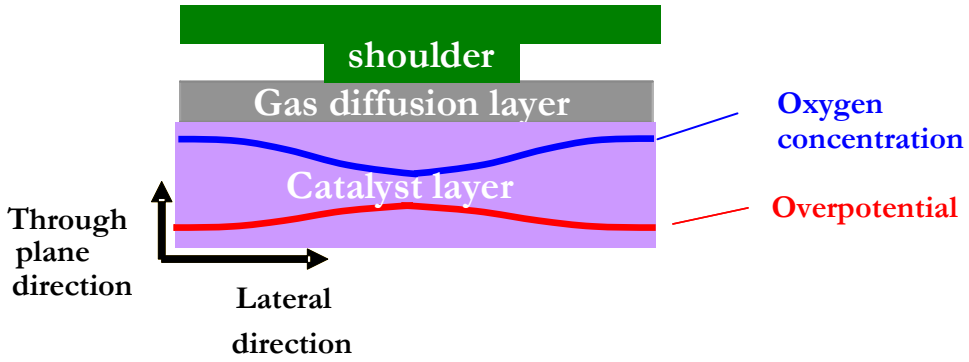

Fig. 2.2. Schematic of the oxygen concentration and overpotential concentration when finite electric conductivity is considered in fuel cell models.

Nguyen et al. (2004), Sivertsen et al. (2005), Lin and Nguyen (2006) and Meng and Wang (2004) considered the gas diffusion layer material is isotropic, so that the electric conductivity in the lateral direction is as same as that in the through-plane direction. These models simulate the current density distribution with different values of electric conductivity in the gas diffusion layer, and concluded that when the electric conductivity becomes low, the average current density is higher under the shoulder than that under the channel due to the low lateral electric conductivity. Yet another study, Zhou and Liu (2006) used a practical value of the electric conductivity in the lateral direction, which is about 14 times larger than the electric conductivity in the through-plane direction. The modeling result shows that for the current GDL materials, their lateral electrical conductivity is not small enough to cause the current density to be higher under the shoulder.

Facing the different modeling results, it is of great significance both academically and practically to know for sure where, under the shoulder or the channel, the current density is higher in a typical PEMFC. Many experiments were carried out to measure the current distribution. However most of them concerned the current density variation either

along the gas channels or in large segments. Hence the objective of this study is to develop a new method to measure the current density under the channel and under the shoulder separately to find out where the current density is higher and how large the difference is. In this experimental study, fuel cells and membrane electrode assemblies are specially designed and fabricated to make the measurement of the current density under the channel or under the shoulder separately possible.

The experiment results show that the current density under the shoulder is higher than that under the channel when the current density of the fuel cell was low. When the fuel cell current density increases to be high, the current density under the shoulder becomes lower than that under the channel. To explain this phenomenon, two sets of experiments have been carried out. One experiment is to test the effect of the lateral electric resistance of the gas diffusion layer on the current density distribution. The other experiment is to measure the through-plane electric resistance of the gas diffusion layer under different compressions, so that the difference of the through-plane electric resistance under the channel and under the shoulder will be estimated.

The experiment shows different current distribution from the modeling results presented by Zhou and Liu (2006). The experimental results indicate the overestimation of difference between the oxygen concentration under the channel and under the channel by the model. The level of the uniformity of the oxygen concentration is affected by the diffusivity of oxygen. Although increasing the oxygen diffusivity may yield a more uniform oxygen distribution across the channel direction, at the same time the limiting current density would be overestimated. Therefore the pseudo-homogeneous model cannot provide an accurate simulation to the catalyst layer. Facing this problem, a new

model of catalyst layer is developed to provide a better simulation of the transport phenomena in the catalyst layer. This model combines the thin-film model [Will (1963A)] and the pseudo-homogeneous model to treat the catalyst layer. Fig. 2.3 shows the schematic of the catalyst layer with a thin Nafion film attached to it. In this model, the oxygen will dissolve and diffuse through a thin Nafion film on each catalyst particles before oxygen reaches the active three-phase surface to participate in the chemical reaction. Some previous modeling works also used the thin-film model [Lin et al. (2004), Wang et al. (2004), Jaouen et al. (2002), Lin and Nguyen (2006), Madhusudana and Rengaswamy (2006)], but they all coupled this model with the agglomerate model. Only Marr and Li (1999) considered the transport process through the thin Nafion film in its pseudo-homogeneous model, however they described this transport by using a low diffusivity of oxygen diffusion instead of modeling the transport process. In this work, a three-dimensional mathematical model employing the new catalyst model is developed. New governing equations are developed to simulate the whole oxygen transport process in the catalyst layer.

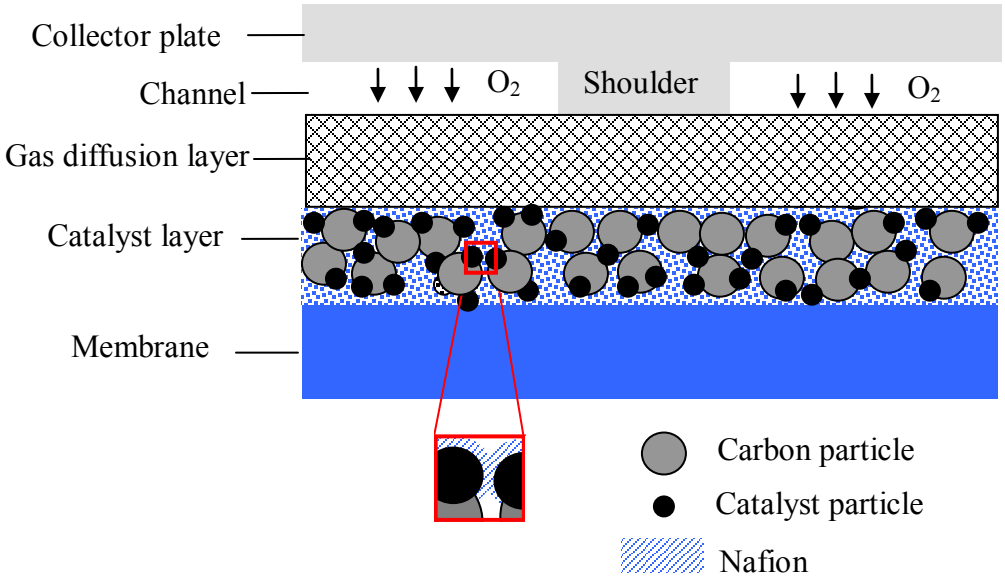

Fig. 2.3 Schematic of the catalyst layer in the model.

CHAPTER 3

EXPERIMENTAL SYSTEM AND PROCEDURE

3.1 Experimental Test Station

The fuel cell test station (FCTS) is manufactured by Fuel Cell Technologies Inc, shown in Fig. 3.1. The test station can control the fuel cell temperature, humidification temperature, pressure and mass flow rate on both the anode and cathode sides. A schematic of the FCTS is shown in Fig. 3.2. The cell temperature and humidification temperature are controlled by the OMEGA CN76000 thermocouple controllers. The reactant gases are humidified by passing through the humidifiers. Regulating the water temperature in the humidifiers controls the gas humidification. Two backpressure regulators at the outlets of the fuel cell are used to control the operating pressure. A computer with a Labview^{TM}-based software controls the MKS mass flow controllers. The amount of mass flow rate is set and read through the software. In each experiment, constant mass flow rate of reactant gases was used instead of constant stoichiometry to get complete polarization curves. The fuel cell polarization curves are obtained by controlling the HP6050 Electronic Load which measures the cell output voltage and current.

Fig. 3.1 Fuel Cell Test Station

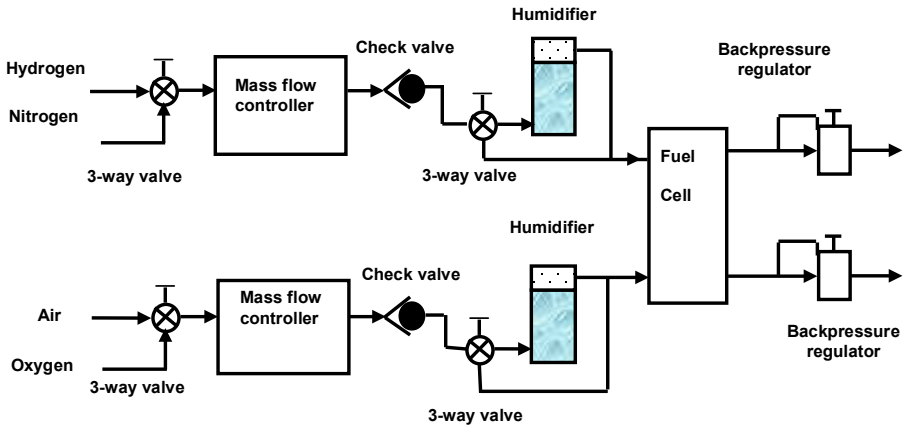

Fig. 3.2 Gas flow path of the fuel cell test station.

The Labview-based software provides an interface not only to set the control conditions for the HP6050A, but also to collect the voltage vs. current data sent back from the HP6050A to draw polarization curves. The interface, "Fuel Cell Testing Program", is shown in Fig. 3.3. The control conditions including maximum and minimum cell voltage for the measurement, voltage step between each two consecutive readings and time delay between readings are all set through this interface. Experimental parameters and some other fuel cell information can be input in this interface, including:

- Fuel cell area
- Number of cells in stack
- Station number – determined by the address of the HP Electronic Load
- Experimental parameters: fuel cell temperature, humidification temperatures, mass flow rates, backpressures.

All these control conditions, fuel cell information, experimental parameters and experimental results of voltage vs. current data will be written to a data file. The path and name of the data file can be set through this interface also.

During each experiment, the measured voltage vs. current data is acquired and plotted on the graph section of the "Fuel Cell Testing Program" interface. Two polarization curves are obtained in each experiment. One curve is recorded when decreasing the voltage from the maximum to the minimum; the other is recorded when increasing the voltage from the minimum back to the maximum.

This software can also record the change of the current and voltage of the fuel cell with time, which is useful for selection of the time delay between readings and breaking in a new fuel cell. The interface is shown in Fig. 3.4.

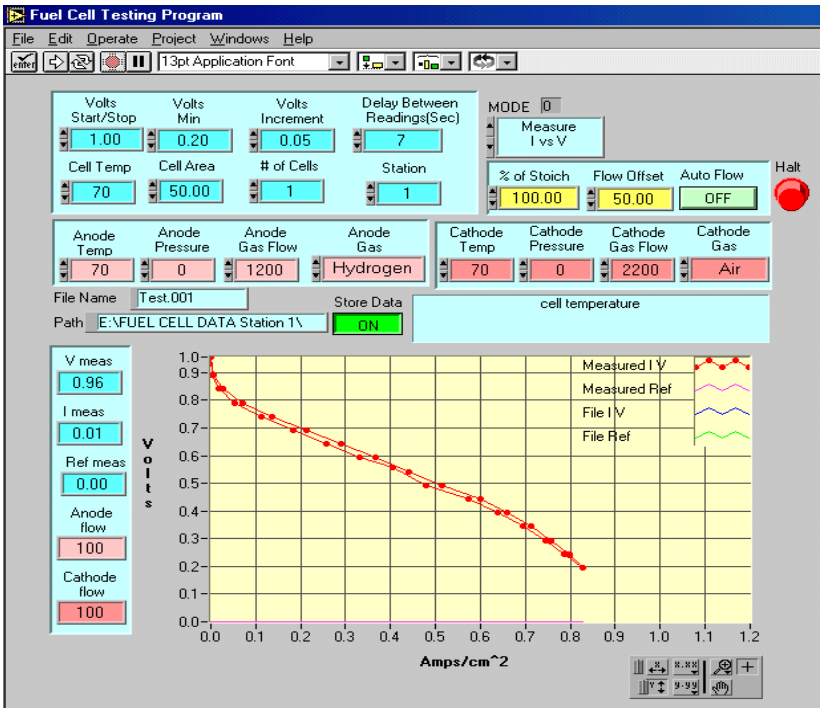

Fig. 3.3 Software interface of "fuel cell testing program".

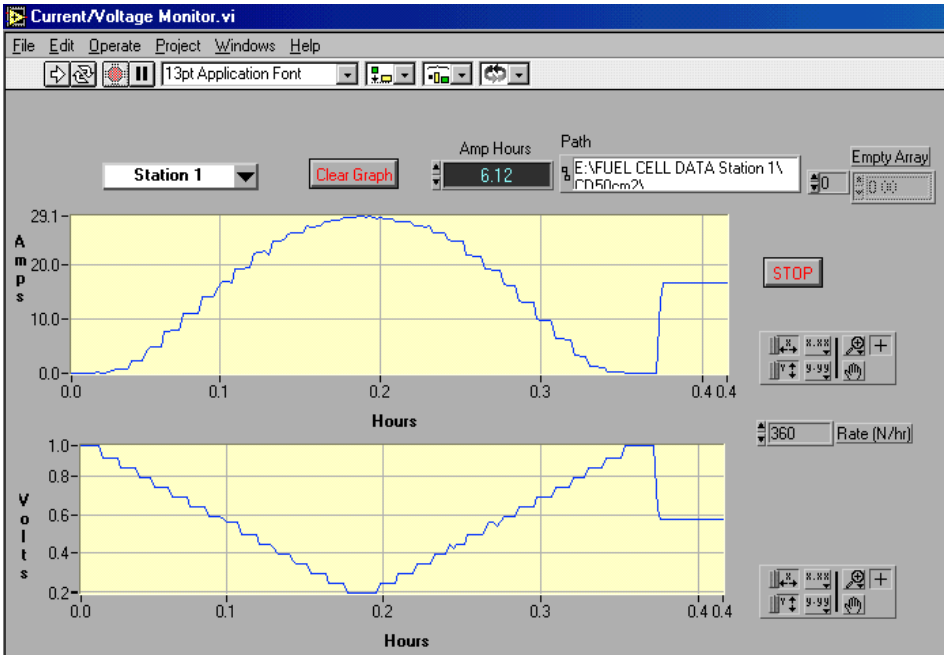

Fig. 3.4 Software interface of "current and voltage monitor"

3.2 Experimental Design

The purpose of the experimental study is to measure the current density distribution under the shoulder and under the channel in the catalyst layer. A parallel cathode collector plate with a special design of flow field is designed and machined for the experiment. The cathode flow field includes only two parallel channels with a shoulder in the middle, shown as in Fig. 3.5. The width of the channels and shoulders are 2mm. Three pieces of MEA with different catalyst distribution are fabricated. One of them has catalyst loaded on the electrode only under the channels, which is used to measure the current produced in the area of catalyst layer under the channels. The electrode under the shoulder contains only carbon. Its configuration is shown in Fig. 3.6(a). Another MEA, shown in Fig. 3.6(b), has catalyst loaded on the electrode only under the shoulder, with which the current produced in the area of catalyst layer under the shoulder is measured. The electrode under the channels contains only carbon. In these two MEAs, the whole electrode has uniform thickness no matter if there is catalyst or not. The last MEA is with a full coverage of catalyst loaded under the two channels and the shoulder, which is used to measure the total current produced by the PEM fuel cell. The configuration of this MEA is shown in Fig.3.6(c).

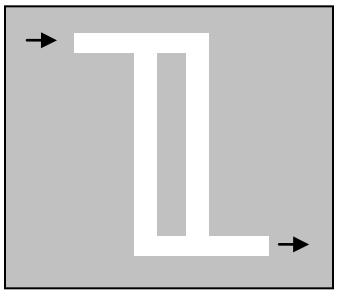

Fig.3.5 Cathode collector plate

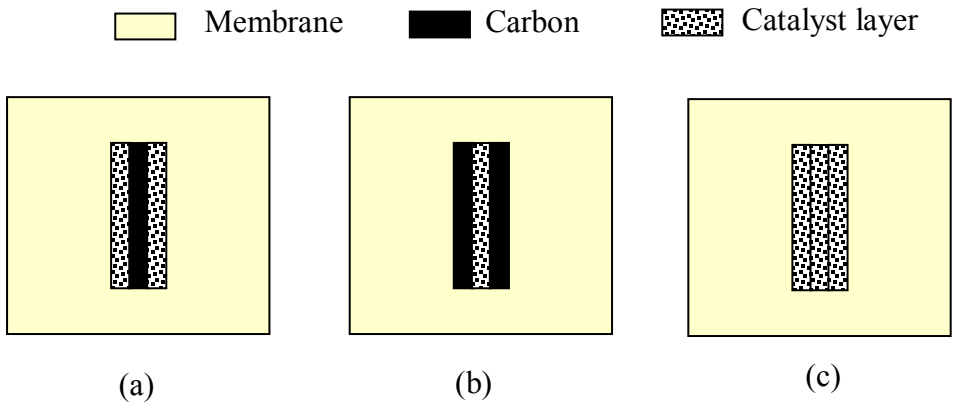

Fig. 3.6 (a) MEA with catalyst under the two channels, (b) MEA with catalyst under the shoulder, (c) MEA with catalyst under the full flow field with two channels and one shoulder.

A series of experiments with four different fuel cell pressures of 1atm, 1.68atm, 2.36atm and 3atm have been done using three PEM fuel cell assemblies with three different MEAs respectively. The cell temperature, humidification temperatures of the anode and cathode sides of the fuel cells are maintained at 70 ºC. The mass flow rate of hydrogen is 1200sccm. The mass flow rate of oxygen is 2200sccm.

The experimental results show that the current density produced in the catalyst layer under the shoulder is higher than the current density produced under the channels when the PEM fuel cell operate under the low current density region. To find out the factors causing the higher current density produced under the shoulder, two more experiments have been carried out. One experiment is to test the effect of lateral electric resistance on the current distribution. A silver mesh is inserted between the collector plate and the GDL in the fuel cell assembly which has the MEA with catalyst coverage under the channels. The cell performance with this fuel cell is tested under four different

pressures, 1atm, 1.68atm, 2.36atm and 3atm. The other experiment is to measure the electron resistance of the GDL under different pressures.

3.3 MEA Preparation

The membrane used in the fuel cell is Nafion® 117 and purchased from Alfa-Aesar Company. The electrodes for the anode and cathode sides are purchased from BCS Fuel Cell Company, made with carbon cloth loaded with catalyst of platinum. The catalyst loading is 0.4 mg/cm^2. The area of the anode electrode is 50cm^2. The area of the cathode electrode is 3.36cm^2. The membrane of Nafion® 117 and the electrodes for the anode and cathode sides are hot-pressed together under the temperature of 120 ºC and pressure of 110lbs/cm^2.

3.4 Fuel Cell Assembly

A single PEMFC assembly is made up of:

- A membrane electrode assembly (MEA)
- A pair of graphite plates on which flow channels are grooved
- A pair of Teflon gaskets for sealing between the MEA and the graphite plates
- A pair of aluminum current collectors
- Two electric wires to connect the fuel cell with the test station to form an electrical circuit
- Two electric wires for measuring of the voltage of the fuel cell

CHAPTER 4

EXPERIMENTAL RESULTS AND DISCUSSION

4.1 Experimental Results of Current Distribution

The experiments for testing the current distribution in PEMFCs are carried out with three different PEM fuel cell assemblies. One fuel cell assembly has a membrane electrode assembly (MEA) with full coverage of catalyst under the flow field. Another one uses a MEA with catalyst loading only under the two channels. The third one uses a MEA with catalyst loading only under the shoulder. For each fuel cell assembly, four tests have been done under different cell pressures, 1atm, 1.68atm, 2.36atm and 3atm.

All the experimental results are presented in the form of polarization curve. The experimental results are compared and analyzed. All the experimental data is also listed in the Appendix.

First of all the current measurement method used in this experiment is validated. The current produced with the MEA which has catalyst only on the electrode under the channels and with the MEA which has catalyst only on the electrode under the shoulder are added together to be compared with the current produced with the regular MEA which has full coverage catalyst in the electrode. The comparison results with different fuel cell pressures are shown in Fig. 4.1 to Fig. 4.4. Under four different fuel cell pressures, the sum of current of the two partly catalyzed MEAs presents matches the current produced by the fuel cell with full catalyst coverage. It proves that the current produced under the channels and under the shoulder using the special designed MEAs are

close enough to represent the current produced under the channel and the shoulder with a normal MEA.

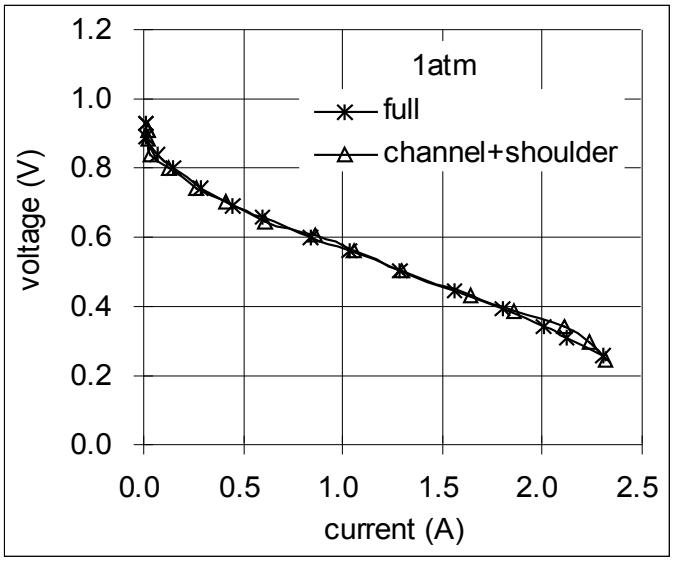

Fig. 4.1. Comparison of current produced by a regular fuel cell and the sum of current produced by two fuel cell with partial loading of catalyst. Anode humidification Temp. = 70°C; Cathode humidification Temp. = 70°C; Hydrogen flow rate = 500sccm; Air flow rate = 2000sccm; Fuel cell pressure = 1atm.

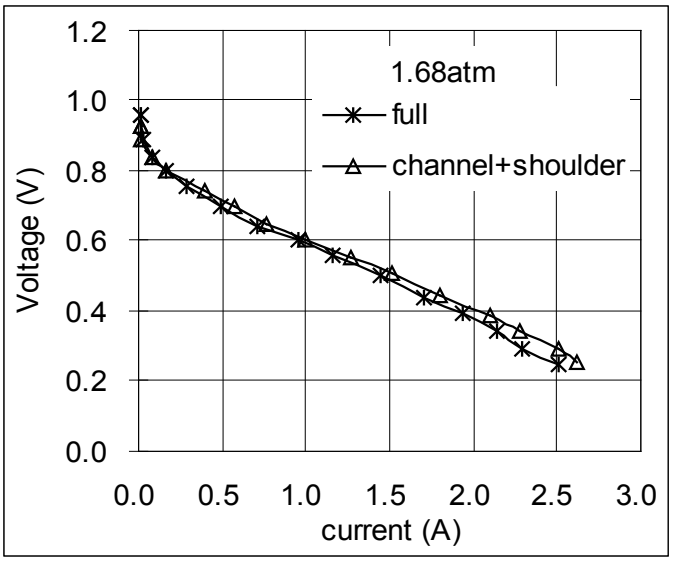

Fig. 4.2 Comparison of current produced by a regular fuel cell and the sum of current produced by two fuel cell with partial loading of catalyst. Anode humidification Temp. = 70°C; Cathode humidification Temp. = 70°C; Hydrogen flow rate = 500sccm; Air flow rate = 2000sccm; Fuel cell pressure = 1.68atm.

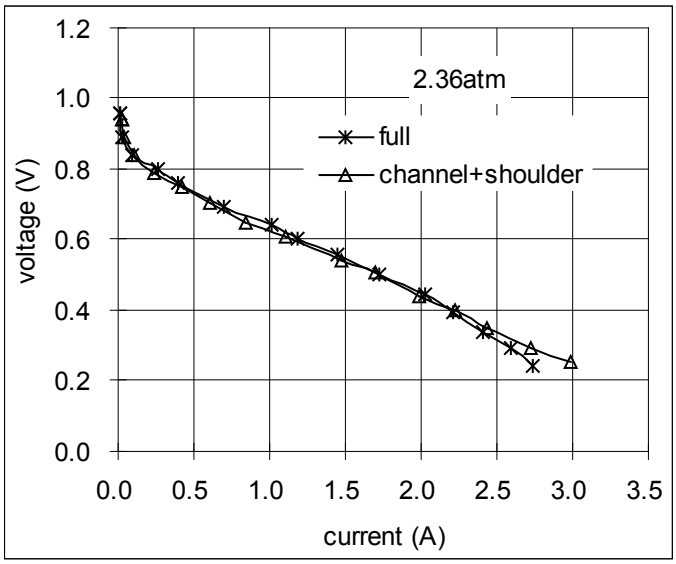

Fig. 4.3. Comparison of current produced by a regular fuel cell and the sum of current produced by two fuel cell with partial loading of catalyst. Anode humidification Temp. = 70°C; Cathode humidification Temp. = 70°C; Hydrogen flow rate = 500sccm; Air flow rate = 2000sccm; Fuel cell pressure = 2.36atm.

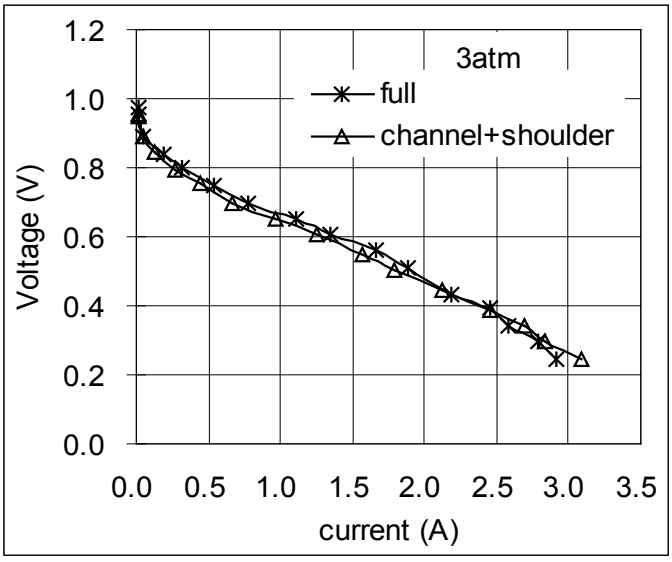

Fig. 4.4. Comparison of current produced by a regular fuel cell and the sum of current produced by two fuel cell with partial loading of catalyst. Anode humidification Temp. = 70°C; Cathode humidification Temp. = 70°C; Hydrogen flow rate = 500sccm; Air flow rate = 2000sccm; Fuel cell pressure = 3atm.

The current density in the catalyst layer under the channels is compared with that under the shoulder. It is shown in Fig. 4.5-4.8 that the current density under the shoulder is higher than the current density under the channel in the low current density region. However with the increase of the current density, the current density under the shoulder becomes lower than that under the channel. This phenomenon can be explained by the alternating dominant factors of mass transport and overpotential. When the current density is low, the mass concentration of reactant gases in the electrode under the channel and the shoulder has little difference, thus the overpotential becomes dominant, therefore higher overpotential under the shoulder leads to higher current density. When the fuel cell is working at high load, the oxygen is consumed fast. The concentration effect becomes dominant. The oxygen concentration in the catalyst layer under the shoulder is significantly lower than that under the channels, thereby leading to higher current density under the channels than that under the shoulder.

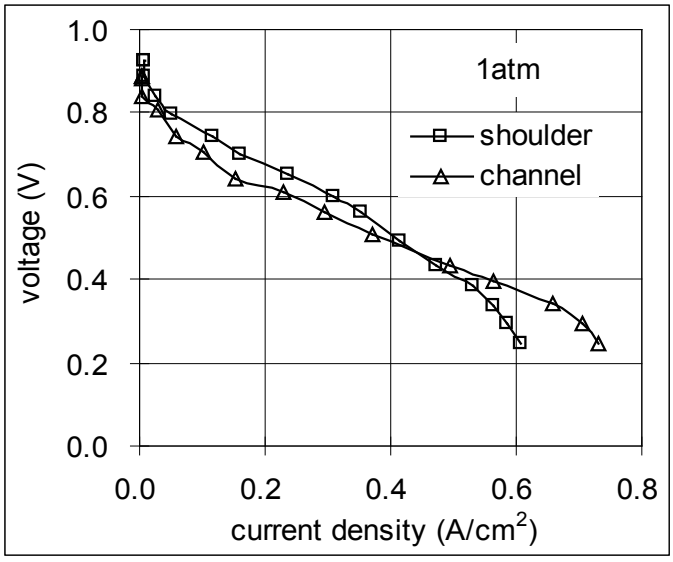

Fig. 4.5 Comparison between current density under the channel and the shoulder . Anode humidification Temp. = 70°C; Cathode humidification Temp. = 70°C; Hydrogen flow rate = 500sccm; Air flow rate = 2000sccm; Fuel cell pressure = 1atm.

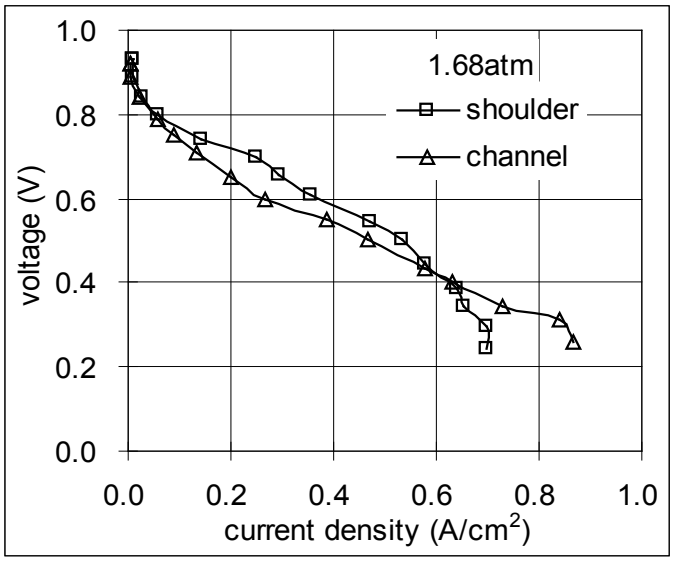

Fig. 4.6 Comparison between current density under the channel and the shoulder. Anode humidification Temp. = 70°C; Cathode humidification Temp. = 70°C; Hydrogen flow rate = 500sccm; Air flow rate = 2000sccm; Fuel cell pressure = 1.68atm.

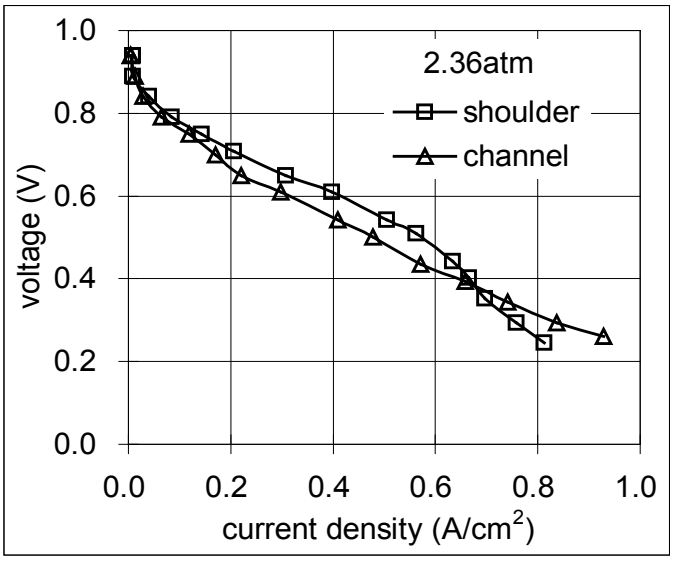

Fig. 4.7 Comparison between current density under the channel and the shoulder . Anode humidification Temp. = 70°C; Cathode humidification Temp. = 70°C; Hydrogen flow rate = 500sccm; Air flow rate = 2000sccm; Fuel cell pressure = 2.36atm.

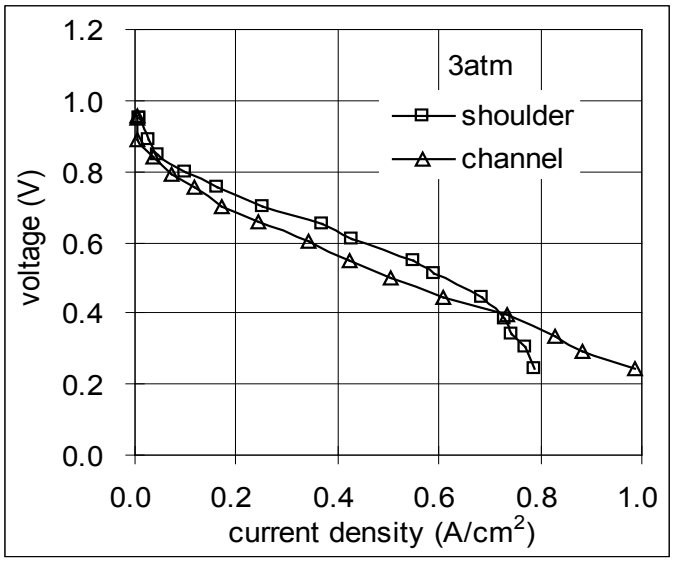

Fig. 4.8 Comparison between current density under the channel and the shoulder. Anode humidification Temp. = 70°C; Cathode humidification Temp. = 70°C; Hydrogen flow rate = 500sccm; Air flow rate = 2000sccm; Fuel cell pressure = 3atm.

4.2 Effect of Lateral Electric Resistance on Current Distribution

The previous modeling results showed that the lateral electric resistance causes the higher current density under the shoulder (Meng and Wang, 2004). To testify the effect of the lateral electric resistance on the current distribution, the experiment is conducted with the PEMFC which has the catalyst loaded only under the channel. The polarization curves with and without the silver mesh under four different operating pressures are compared and displayed in Fig. 4.9-12. Under the pressures of 1atm, 1.68atm, 2.36atm and 3atm, the fuel cell performance does not show apparent improvement with the silver mesh, which indicates that the lateral electric resistance does not cause the non-uniform overpotential across the channel and shoulder direction. Accordingly it is inferred that the different through-plane electric resistance under the channel and the shoulder makes the higher overpotential

under the shoulder.

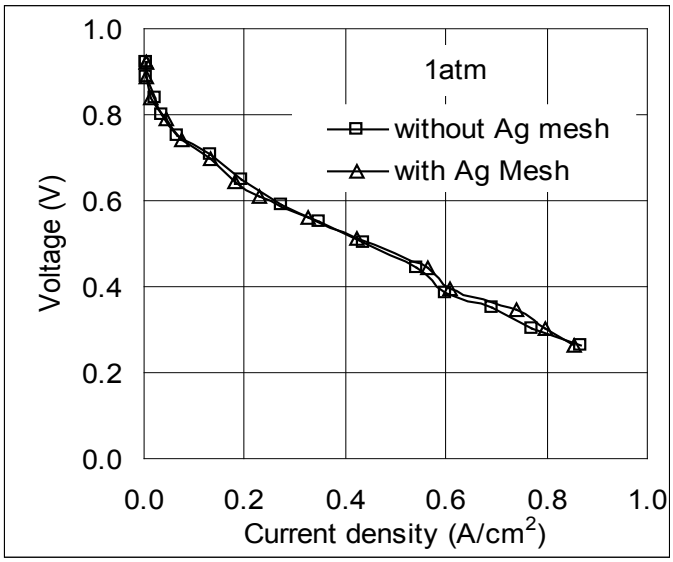

Fig. 4.9. Comparison between current density with and without Ag mesh under the channel. Anode humidification Temp. = 70°C; Cathode humidification Temp. = 70°C; Hydrogen flow rate = 500sccm; Air flow rate = 2000sccm; Fuel cell pressure = 1atm.

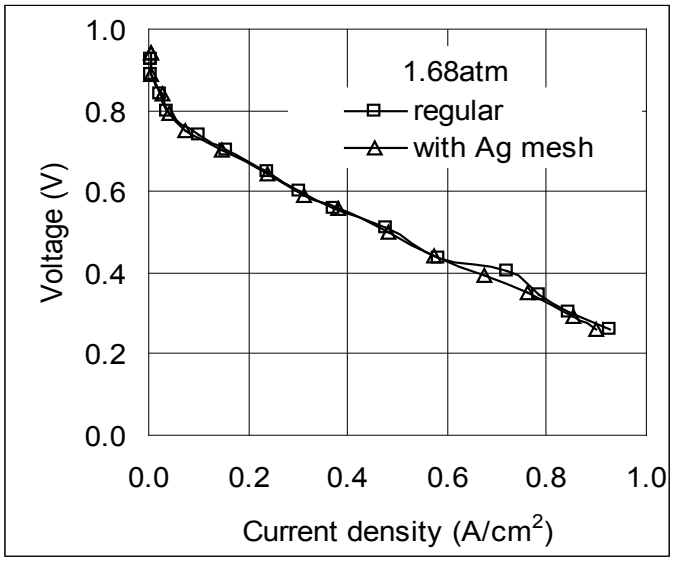

Fig. 4.10. Comparison between current density with and without Ag mesh under the channel. Anode humidification Temp. = 70°C; Cathode humidification Temp. = 70°C; Hydrogen flow rate = 500sccm; Air flow rate = 2000sccm; Fuel cell pressure = 1.68atm.

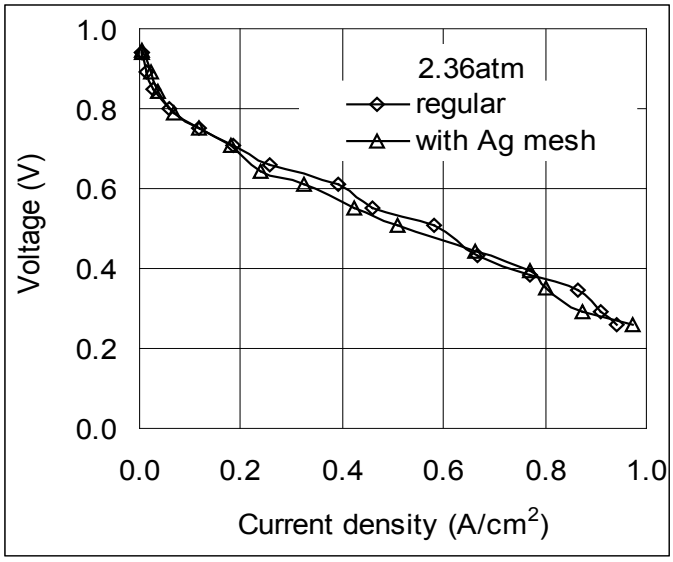

Fig. 4.11. Comparison between current density with and without Ag mesh under the channel. Anode humidification Temp. = 70°C; Cathode humidification Temp. = 70°C; Hydrogen flow rate = 500sccm; Air flow rate = 2000sccm; Fuel cell pressure = 2.36atm.

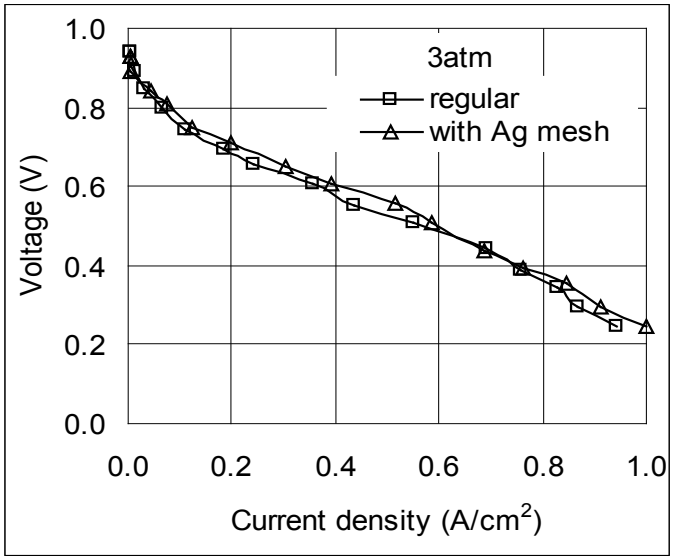

Fig. 4.12. Comparison between current density with and without Ag mesh under the channel. Anode humidification Temp. = 70°C; Cathode humidification Temp. = 70°C; Hydrogen flow rate = 500sccm; Air flow rate = 2000sccm; Fuel cell pressure = 3atm.

4.3 Effect of Contact Resistance on Current Distribution

The through-plane electric resistance is measured under different pressures. The experimental result is shown in Fig. 4.13.

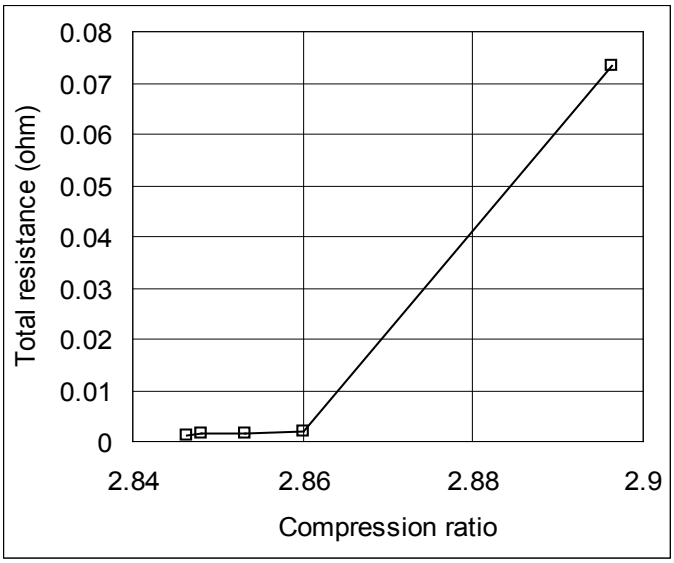

Fig. 4.13. Through-plane electric resistance of electrode under different compressions.

In this experiment, the compression is represented by the distance between the two plate pressed on the electrode. The larger the distance, the less the compression exerted on the electrode. The electric resistance is measured under five different compressions. When there is no force exerted on the plates, which simulate the situation of the part of the electrode under the channel, the through-plane electric resistance is 7.3 mΩ. When the compression is 15 lbf, which is added on the part of the electrode under the shoulder, the electric resistance is 1 mΩ. The difference of the through-plane electric resistance of the electrode under the channel and under the shoulder is significant, which will lead to the difference of the overpotential under the channel and under the shoulder.

CHAPTER 5

MODEL DEVELOPMENT AND MODELING STUDY ON CURRENT DISTRIBUTION IN A PEMFC

5.1 Model Description

5.1.1 Background

A comprehensive three-dimensional model for PEM fuel cells is developed to study the mass transport and electron transport in a PEM fuel cell. The catalyst layer is modeled in a new way by combining the thin-film model and the homogeneous model. Since the energy loss of a PEM fuel cell largely comes from the cathode side for the slow reaction rate of the oxygen reduction, the model includes the cathode side of a PEMFC only. The model domain, shown in Fig. 5.1 includes a flow field containing a gas channel and half of a shoulder, a gas diffusion layer, a catalyst layer and a membrane.

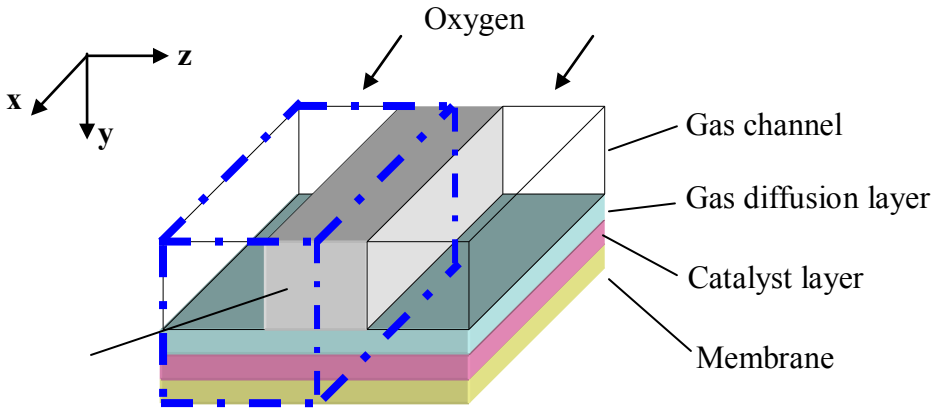

Fig. 5.1 The 3-D geometric model of a single PEM fuel cell.

In the 3-D mathematical model, governing equations of continuity, momentum, species concentrations and phase potential are coupled to be solved. The chemical reaction of the oxygen reduction at the cathode side is simulated by different source terms into the governing equations. The domain of the continuity, momentum and species concentration equations include a flow field, a gas diffusion layer and a catalyst layer at the cathode side. The domain of the solid-phase potential equation includes a gas diffusion layer and a catalyst layer. The domain of the electrolyte-phase potential equation includes a catalyst layer and a membrane. The domain for each governing equation is considered as an entirety. The advantage of this treatment is that the boundary conditions at the interfaces of different cell components in a domain do not need to be specified, which makes the model simplified and increases the accuracy of the model.

5.1.2 Model assumptions

The assumptions used by the 3-D mathematical model are listed below:

1. The gas mixtures are considered to be perfect gases and are incompressible.
2. The liquid water volume occupied in the gas channels, gas diffusion layers and catalyst layers is negligible.
3. The flow is laminar.
4. Only the steady-state case is considered.
5. The fluid properties are assumed to be constant.
6. The gas diffusion layers, catalyst layers and the membrane are considered as isotropic porous media.

5.1.3 Mathematical model

To clarify the mathematical model, the governing equations are listed.

- *Continuity equation*

The continuity equation for the domain of the flow field, gas diffusion layer and catalyst layer is listed in Eq. 5.1:

$$\frac{\partial u}{\partial x}+\frac{\partial v}{\partial y}+\frac{\partial w}{\partial z}=\begin{cases}0 & \text{channel, gas diffusion layer}\\ S_k & \text{catalyst layer}\end{cases} \tag{5.1}$$

where S_k is the consumption or production of the species in the catalyst layer, which is defined later in the species equations.

- *Momentum equation*

The momentum transport of the reactant gas in a PEMFC is governed by the Navier-Stokes equations. In the gas diffusion and catalyst layers, which are porous media, the Darcy's force is added in the equation accounting for the force exerted on the reactant gas by the solid interface of the pores [Dagan, 1989]. They are listed below respectively:

$$\rho\vec{\mathrm{u}}\cdot\left(\nabla\vec{\mathrm{u}}\right)=-\nabla p+\mu\nabla^2\vec{\mathrm{u}} \qquad \text{(gas channel)} \tag{5.2}$$

$$\rho\vec{\mathrm{u}}\cdot\left(\nabla\vec{\mathrm{u}}\right)=-\nabla p+r^{(2)}\mu\nabla^2\vec{\mathrm{u}}-\frac{\varepsilon\mu}{k_p}\vec{\mathrm{u}} \qquad \text{(gas diffusion layer, catalyst layer)} \tag{5.3}$$

k_p is the permeability of the gas mixtures in the graphic porous medium. The porous media correction factor $r^{(2)}$ in the momentum equations is defined as (Dagan, 1979):

$$r^{(2)}=\frac{2.25(1-\varepsilon)^2}{\varepsilon^2} \tag{5.4}$$

- *Species equation*

The reactant gas is transported by diffusion and locally by convection in the gas channel and the diffusion layer. The mass transport of the reactant gas is governed by the species equation. The equations for different component in the domain are listed below:

$$\vec{u} \cdot \nabla C_k = D_{eff} \nabla^2 C_k \qquad \text{(gas channel and diffusion layer)} \qquad (5.5)$$

$$\vec{u} \cdot \nabla C_k = D_{eff} \nabla^2 C_k + S_k \qquad \text{(catalyst layer)} \qquad (5.6)$$

$D_{eff,k}$ is the porous media effective diffusivity, which is taken as (Bernardi and Verbrugge, 1991):

$$D_{eff,k} = D_k \ \varepsilon_g^{1.5} \qquad (5.7)$$

D_k is the diffusivity of a species k. The diffusivity of oxygen in the porous media is determined by the correlation from Ogumi et al. (1984):

$$D_{O_2} = 3.1 \times 10^{-3} \exp(-\frac{2768}{T}) \qquad (5.8)$$

In the species equation of the catalyst layer, the last term S_k represents production or consumption of the species caused by the chemical reaction in the catalyst layer. For the oxygen and water at the cathode, the source terms S_k respectively are: $\frac{j_c}{4F}, -\frac{j_c}{2F}, j_c$ is the volumetric current produced in the catalyst layer.

- *Transport of oxygen in the catalyst layer*

In this model, the transport of oxygen to the active site in the catalyst layer has two steps. The first step is to transport from the diffusion layer to the catalyst layer through the pores by diffusion and convection, which is governed by the species equation (5.5) and (5.6). The second step is the diffusion of dissolved oxygen through the Nafion

films attached on the catalyst surfaces. The schematic of the environment for this procedure is shown in Fig. 5.2.

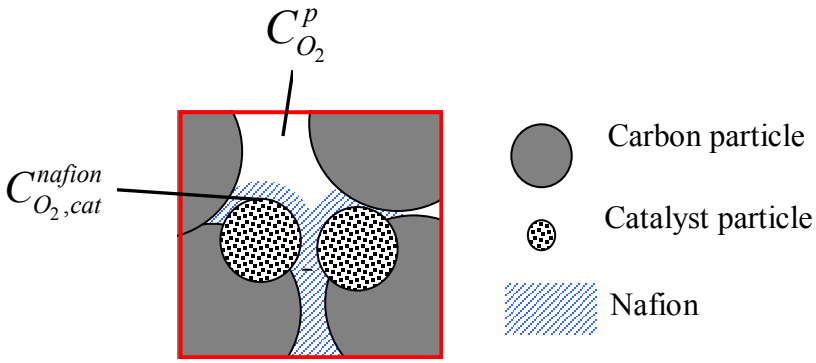

Fig. 5.2 Schematic of three-phase reactions site

Arriving at the surface of the Nafion film, oxygen will dissolve into the Nafion and the concentration will be reduced, which is governed by Henry's Law. Hence at the surface of the Nafion film, the concentration of the dissolved oxygen is:

$$C_{O_2,0}^{nafion} = HC_{O_2}^{p} \tag{5.9}$$

where $C_{O_2}^{p}$ is the oxygen concentration in the pores, $C_{O_2,0}^{nafion}$ is the concentration of the dissolved oxygen on the surface of the Nafion film, and H is Henry's Constant. Then the dissolved oxygen will diffuse through the film to the catalyst surface. Because the Nafion film is so thin that the diffusion process is considered to be one-dimensional and governed by the Fick's Law:

$$D_{O_2}^{nafion} \frac{C_{O_2,0}^{nafion} - C_{O_2,cat}^{nafion}}{\delta_{nafion}} = \frac{i_c}{4F} \tag{5.10}$$

where $C_{O_2,cat}^{nafion}$ is the concentration of dissolved oxygen on the surface of the catalyst particle, i_c is the current density produced on the active surface on catalyst particles, which is calculated from Butler-Volmer equation:

$$i_c = i_0^{ref}\left(\frac{C_{O_2,cat}^{nafion}}{C_{O_2}^{ref}}\right)\left(-e^{-\frac{\alpha_c^c F}{RT}\eta_c}\right) \tag{5.11}$$

i_0^{ref} is the exchange current density, which is determined by the correlation obtained from the experimental results of Parthasarathy et al. (1992):

$$\log_{10}(i_0^{ref}) = 3.507 - \frac{4001}{T} \tag{5.12}$$

The relationship of the volumetric current production j_c and i_c is expressed as:

$$j_c = a i_c \tag{5.13}$$

where a is the active catalyst surface area per unit volume of the catalyst layer.

In the equation (5.11), η_c is the overpotential, which is defined as the departure of the potential difference of the two phases from the potential difference at the equilibrium condition.

$$\eta_c = (\phi_s - \phi_e) - E_0 + \int iR_m + \int (I - i)R_s \tag{5.14}$$

Since ϕ_s and ϕ_e are the actual potential of the solid and electrolyte phase obtained by considering both the ohmic loss and the activation loss, then the departure of the potential difference from the equilibrium potential difference include both the overpotential and the ohmic voltage drop. Consequently the contribution of the ohmic voltage drop to the potential difference departure should be excluded.

- *Potential equation*

In this model, the electron transport and ion transport are considered; therefore the potentials of the solid phase and the membrane phase are not constant. The membrane phase potential is calculated in the membrane and the catalyst layer, the potential equation is:

$$\frac{\partial}{\partial x}(\sigma_p \frac{\partial \phi_p}{\partial x}) + \frac{\partial}{\partial y}(\sigma_p \frac{\partial \phi_p}{\partial y}) + \frac{\partial}{\partial z}(\sigma_p \frac{\partial \phi_p}{\partial z}) = \begin{cases} -j_c & \text{Catalyst layer} \\ 0 & \text{Membrane} \end{cases} \tag{5.15}$$

The solid phase potential is calculated in the gas diffusion and catalyst layer, the potential equation is:

$$\frac{\partial}{\partial x}(\sigma_{e,xz} \frac{\partial \phi_e}{\partial x}) + \frac{\partial}{\partial y}(\sigma_{e,y} \frac{\partial \phi_e}{\partial y}) + \frac{\partial}{\partial z}(\sigma_{e,xz} \frac{\partial \phi_e}{\partial z}) = \begin{cases} j_c & \text{Catalyst layer} \\ 0 & \text{Gas diffusion layer} \end{cases} \tag{5.16}$$

note that $j_c \le 0$.

Since the electric conductivities in the through-plane and the in-plane directions of carbon cloth, a commonly used gas diffusion layer, have significant difference, the electric conductivities in two directions of the gas diffusion layer are considered.

5.1.4 Boundary conditions

Boundary conditions for the momentum, species equations

The modeling domain of momentum transport and mass transport includes a flow channel, a gas diffusion layer, a catalyst layer on the cathode side. It is assumed that all parameters are continuous between interfaces between any two layers. Therefore the boundary conditions are needed only on the boundaries of the domain, not on any interfaces between any two layers. The schematic of the boundary conditions for the momentum and species equations are shown in Fig. 5.3. The inlet conditions of the

reactant gas are given at the inlet of the channel, such as the velocity and concentration. At the gas channel walls, the interface between the catalyst layer and the membrane, and all other boundaries, the Neumann condition is applied, as gas is impermeable through these boundaries.

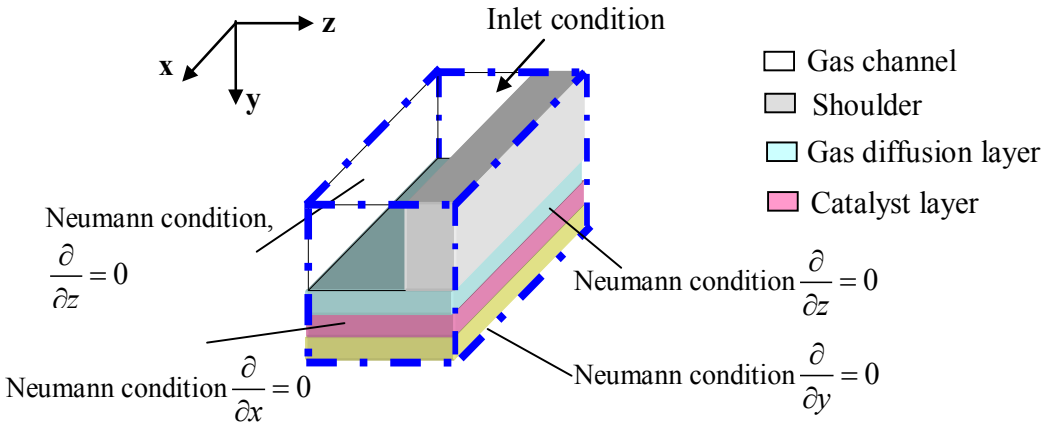

Fig. 5.3 Schematic of the boundary conditions on the domain of the momentum and mass transport modeling.

For the modeling of membrane phase potential, the domain includes the catalyst layer and membrane. Protons can be conducted through the gas diffusion layer, therefore the Neumann condition is applied on the boundary of the catalyst layer. On the boundary of the membrane which connects to the anode catalyst layer, the potential is assumed to be zero. The schematic of the boundary conditions for the membrane phase modeling domain is shown in Fig. 5.4.

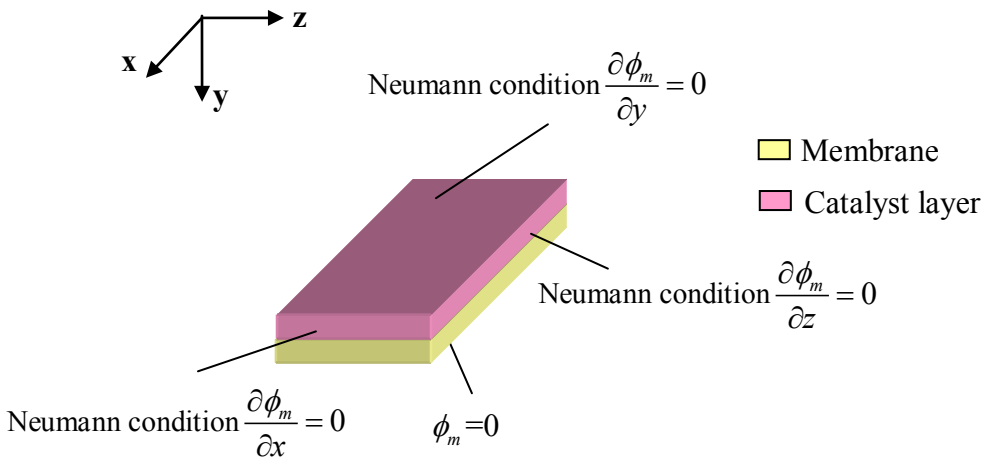

Fig. 5.4 The schematic of the boundary conditions for the membrane phase modeling domain.

For the modeling of solid phase potential, the domain includes the gas diffusion layer and catalyst layer. Electrons cannot be conducted through the membrane, therefore the Neumann condition is applied at the boundary of the interface between the catalyst layer and the membrane. The boundary of the gas diffusion layer connecting to the collector plate, the solid phase potential is assumed to be equal to the cell voltage. Although the actual potential on this surface should be less than the cell voltage because of the ohmic loss of the electron transport through the collector plate, the electric conductivity of the collector plate is so high that the ohmic loss can be neglected. The Neumann condition is applied to all other boundaries of the domain, since electrons cannot be transported through. The schematic of the boundary conditions for the membrane phase modeling domain is shown in Fig. 5.5.

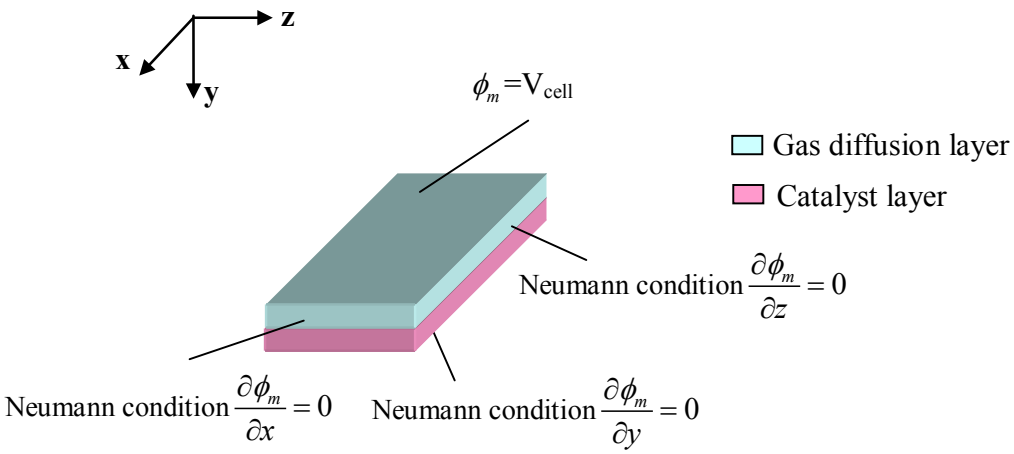

Fig. 5.5 The schematic of the boundary conditions for the membrane phase modeling domain.

5.2 Numerical Scheme

The mathematical model is developed using FORTRAN language. The general differential equations are discretized by the control-volume based on the finite difference method of Patankar (1980), and the set of algebraic equations are iteratively solved. The solutions of the velocity component of the equations are obtained in a staggered control volume. The Semi-Implicit method for Pressure-Linked Equations Revised (SIMPLER) algorithm (Patankar, 1980) is used for pressure correction. The rectangular physical domain is divided by a nonuniform grid. The criterion of convergence is that relative change of the value of every unknown between the consecutive two iterations is less than 10^{-5}.

5.3 Modeling Results

5.3.1 Modeling results with different through-plane electric conductivity

From the experimental results, it is found that the through-plane conductivity of the gas diffusion layer under the channel is different from that under the shoulder because of different compressions. Therefore the difference of the through-plane electric conductivity is considered in this model.

Comparison of the polarization curves with experimental results

Firstly the model is verified with the experimental data obtained from the experimental study presented in Chapter 4. The polarization curves calculated from the model are compared with the experimental data. Four polarization curves with different operating pressures of 1atm, 1.68atm, 2.36atm and 3atm are calculated. The comparison results are shown in Fig. 5.6 to Fig. 5.9. The modeling results show a good agreement with the experimental data, which indicates that the mathematical model is valid to simulate a PEM fuel cell.

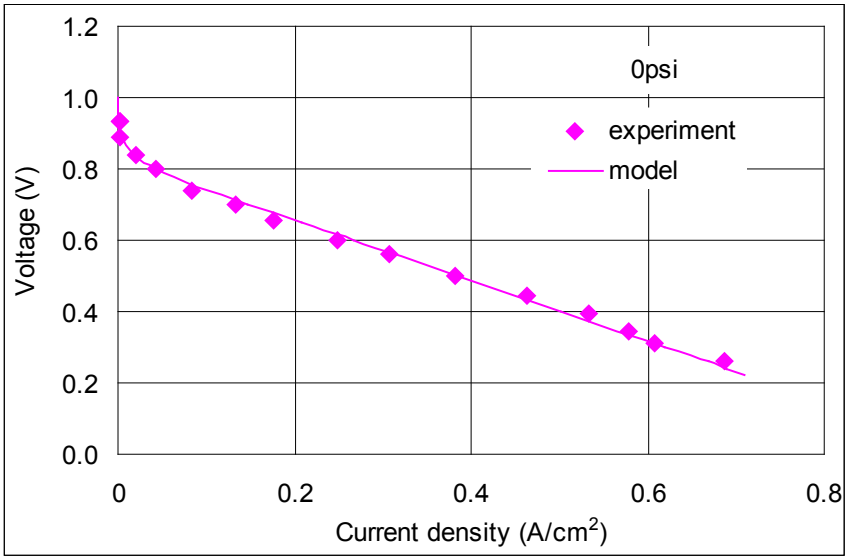

Fig. 5.6 Comparison of the modeling results with the experimental data. Anode humidification Temp. = 70°C; Cathode humidification Temp. = 70°C; Hydrogen flow rate = 500sccm; Air flow rate = 2000sccm; Fuel cell pressure = 1atm.

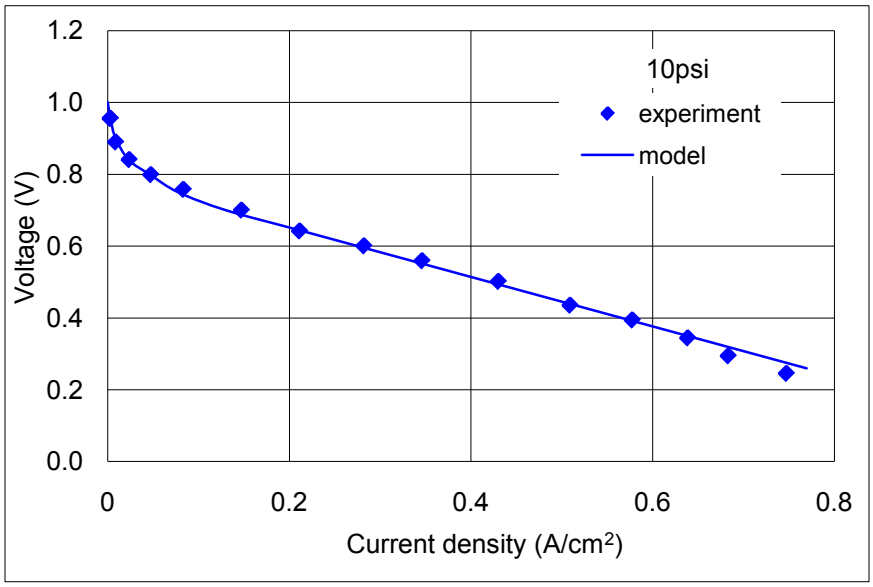

Fig. 5.7 Comparison of the modeling results with the experimental data. Anode humidification Temp. = 70°C; Cathode humidification Temp. = 70°C; Hydrogen flow rate = 500sccm; Air flow rate = 2000sccm; Fuel cell pressure = 1.68atm.

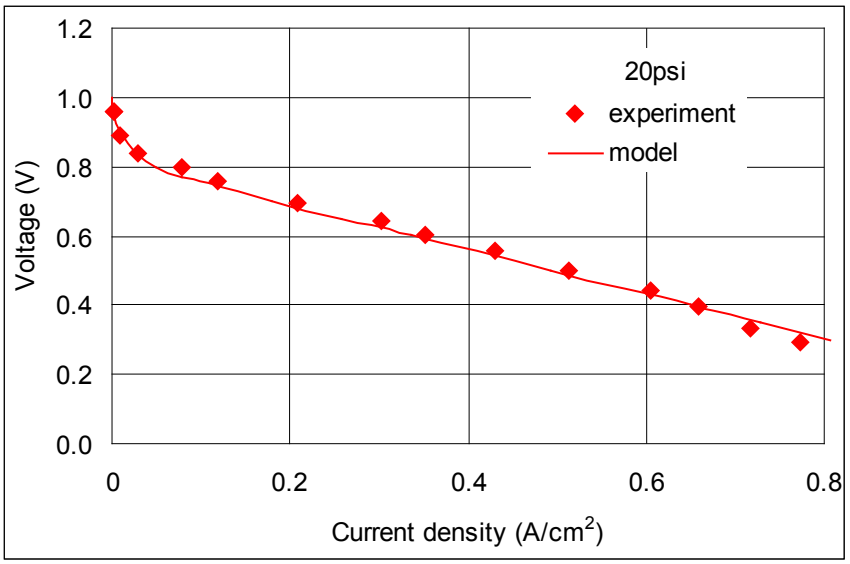

Fig. 5.8 Comparison of the modeling results with the experimental data. Anode humidification Temp. = 70°C; Cathode humidification Temp. = 70°C; Hydrogen flow rate = 500sccm; Air flow rate = 2000sccm; Fuel cell pressure = 2.36atm.

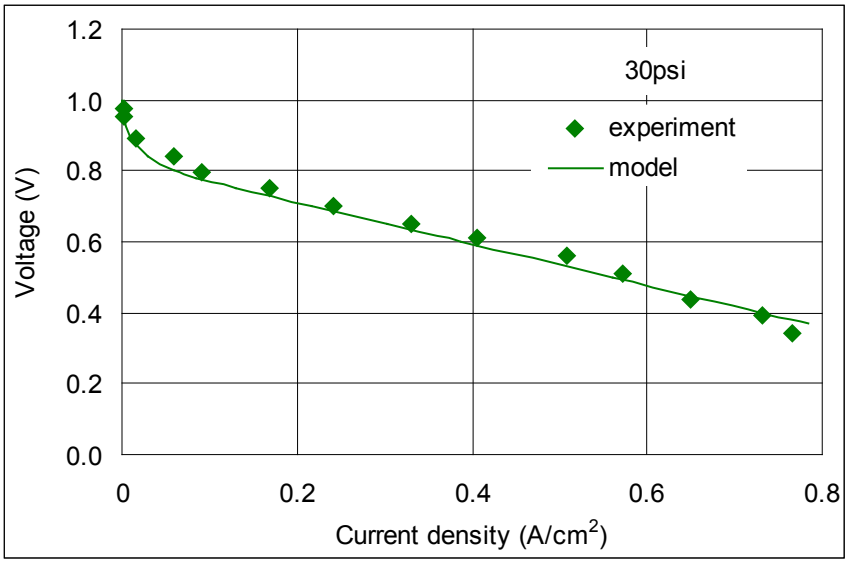

Fig. 5.9 Comparison of the modeling results with the experimental data. Anode humidification Temp. = 70°C; Cathode humidification Temp. = 70°C; Hydrogen flow rate = 500sccm; Air flow rate = 2000sccm; Fuel cell pressure = 3atm.

Current density distribution

The current density distribution has been simulated under the experimental condition of 1atm operation pressure. The current distributions at voltage of 0.6V and 0.25V are shown in Fig. 5.10 and 5.11 respectively. The distribution in the catalyst layer is shown along the gas flow direction and across channel direction. The current density distribution in the catalyst layer when the cell voltage is 0.6 V is shown in Fig. 5.10. It shows that the maximum current density is located above the edge between the channel and the shoulder. The average current density under the shoulder is higher than that under the channel. The modeling results show that the current density under the channel and shoulder are 0.21 A/cm^2 and 0.32 A/cm^2 respectively, which provide good simulations to the experimental results of 0.23 A/cm^2 and 0.31A/cm^2 respectively. The higher current density under the shoulder is caused by the higher through-plane electric resistance of the gas diffusion layer. The current distribution with the cell voltage of 0.26 shows the higher current density under the shoulder, because of the large oxygen concentration difference between the channel and the shoulder.

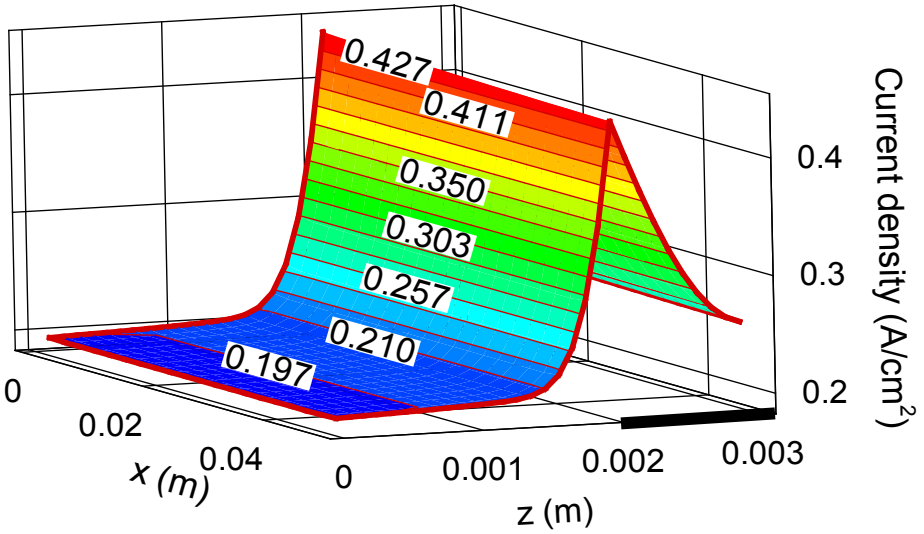

Fig. 5.10 Current density distribution in the catalyst layer. V=0.6V. Anode humidification Temp. = 70°C; Cathode humidification Temp. = 70°C; Hydrogen flow rate = 500sccm; Air flow rate = 2000sccm; Fuel cell pressure = 1atm.

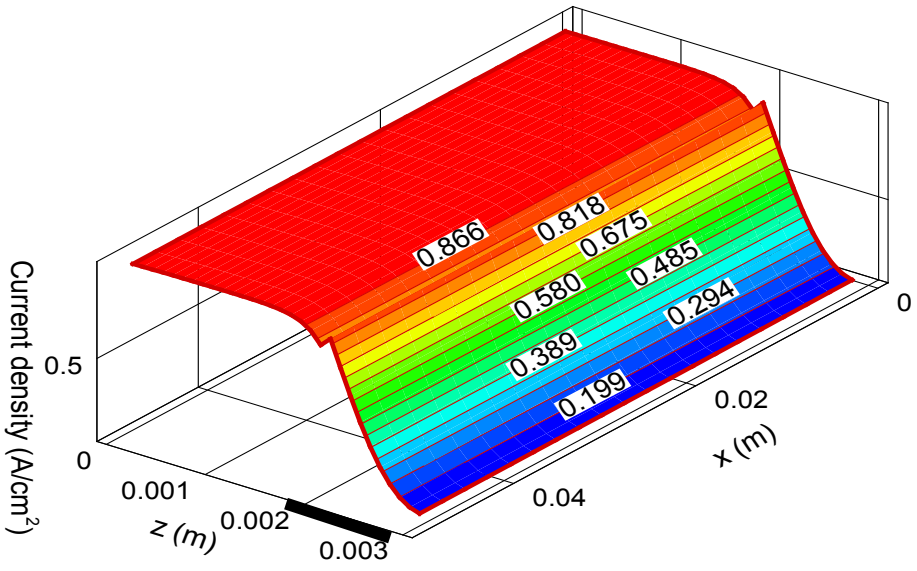

Fig. 5.11 Current density distribution in the catalyst layer. V=0.25V. Anode humidification Temp. = 70°C; Cathode humidification Temp. = 70°C; Hydrogen flow rate = 500sccm; Air flow rate = 2000sccm; Fuel cell pressure = 1atm.

Oxygen Concentration distribution

In this model, the oxygen transport in the catalyst layer experiences two steps. The transport of oxygen through the pores to the surface of Nafion films is followed by the dissolution and diffusion of oxygen through the Nafion films wrapped around the catalyst particles. The simulation results of the oxygen concentration distribution in the pores and in the Nafion film in the catalyst layer are shown in Fig. 5.12 to Fig. 5.17. It is shown that the oxygen concentration under the shoulder is always lower than that under the channel. However the oxygen concentration after the diffusion through the Nafion films is more uniform. This phenomenon is displayed more clearly in the Fig. 5.14 and Fig. 5.17, where the oxygen concentration along the across-channel direction of the transport in the pores and after the diffusion through the membrane has been compared. The more uniform oxygen concentration across the channel direction after the diffusion of Nafion film enables the model to simulate the real operation of PEM fuel cells, which has higher current density under the shoulder at the low load.

It is also observed from Fig. 5.14 and Fig. 5.17 that the oxygen concentration after the diffusion through the Nafion film is more uniform at 0.6V than at 0.26V. Since at 0.26V, the larger current production makes the consumption of oxygen much faster than the rate of oxygen transport, thereby increasing the difference of oxygen concentration under the shoulder and under the channel. The big difference of oxygen concentration under the channel and under the shoulder at the low voltage becomes dominant in determining current distribution across the channel direction. Accordingly the current density is lower under the shoulder than under the channel.

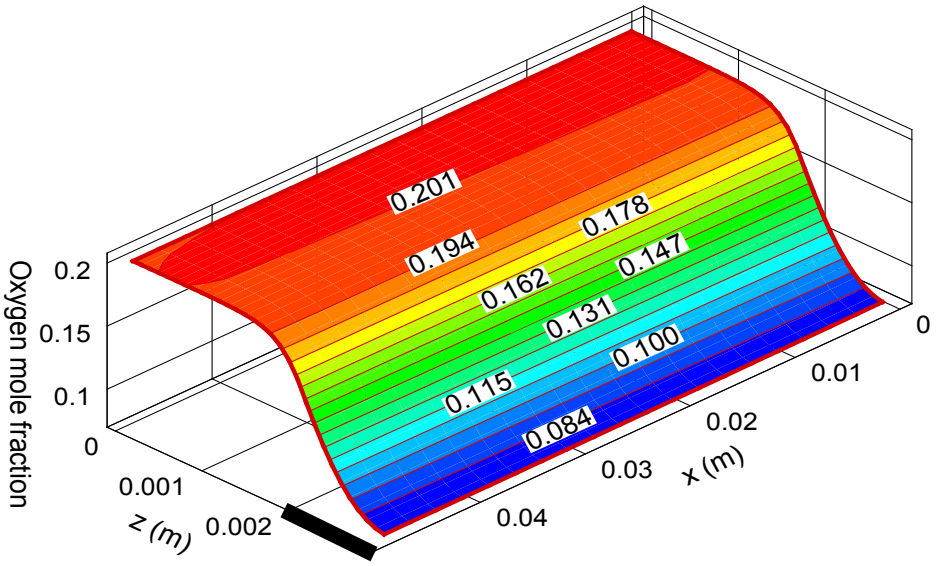

Fig. 5.12 Oxygen concentration distribution in the pores in the catalyst layer. V=0.6V. Anode humidification Temp. = 70°C; Cathode humidification Temp. = 70°C; Hydrogen flow rate = 500sccm; Air flow rate = 2000sccm; Fuel cell pressure = 1atm.

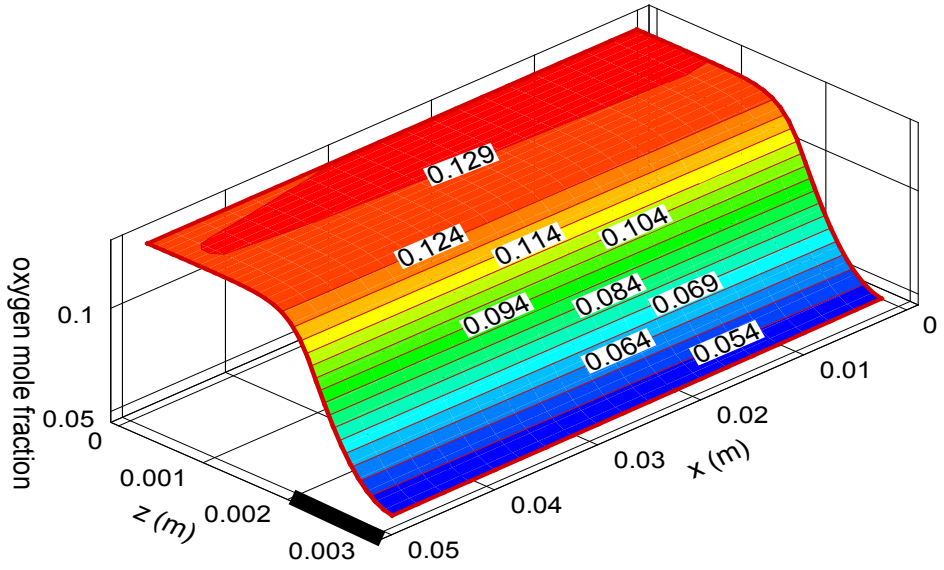

Fig. 5.13 Oxygen concentration distribution after diffusion through the membrane film in the catalyst layer. V=0.6V. Anode humidification Temp. = 70°C; Cathode humidification Temp. = 70°C; Hydrogen flow rate = 500sccm; Air flow rate = 2000sccm; Fuel cell pressure = 1atm.

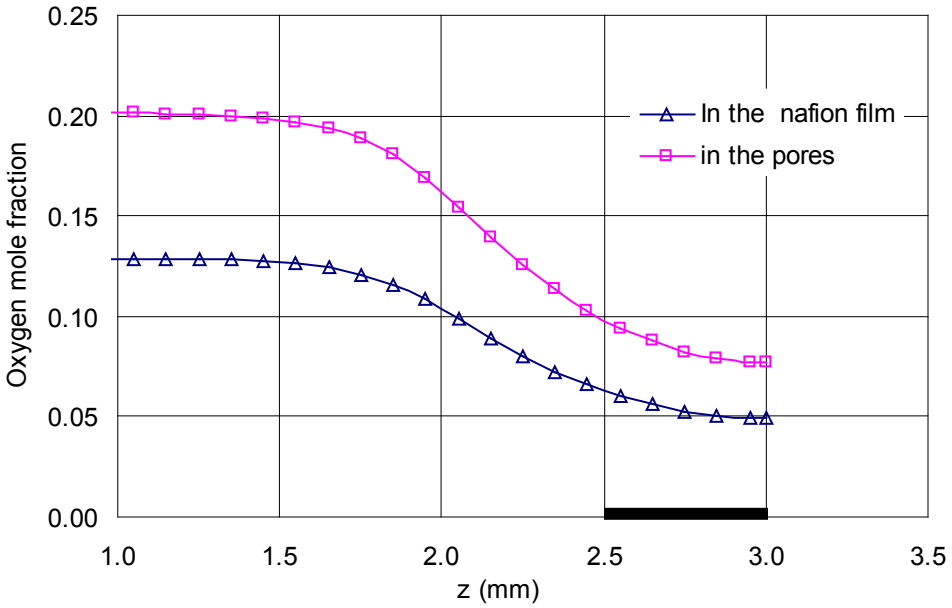

Fig. 5.14 Comparison of oxygen concentration distribution before and after diffusion through the membrane film in the catalyst layer. V=0.6V. Anode humidification Temp. = 70°C; Cathode humidification Temp. = 70°C; Hydrogen flow rate = 500sccm; Air flow rate = 2000sccm; Fuel cell pressure = 1atm. (x/L=0.5)

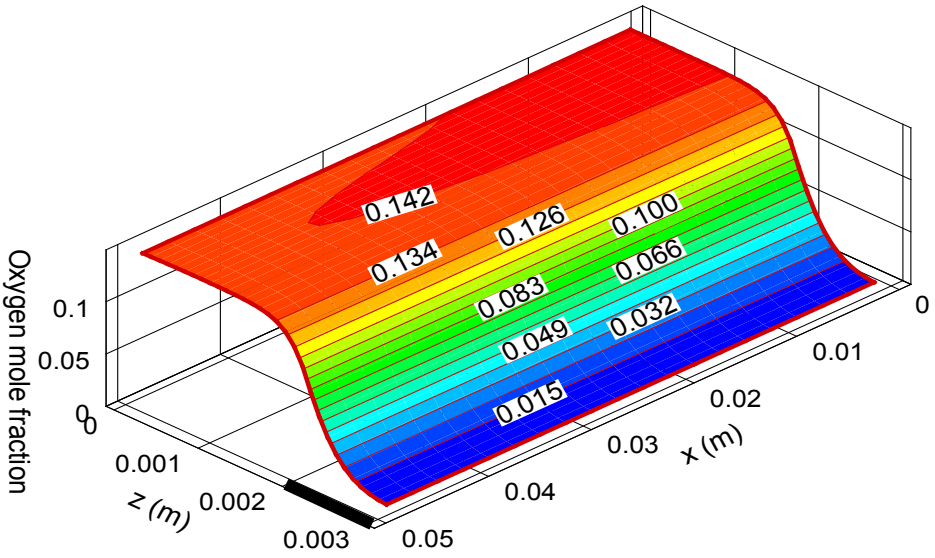

Fig. 5.15 Oxygen concentration distribution in the pores in the catalyst layer. V=0.25V. Anode humidification Temp. = 70°C; Cathode humidification Temp. = 70°C; Hydrogen flow rate = 500sccm; Air flow rate = 2000sccm; Fuel cell pressure = 1atm.

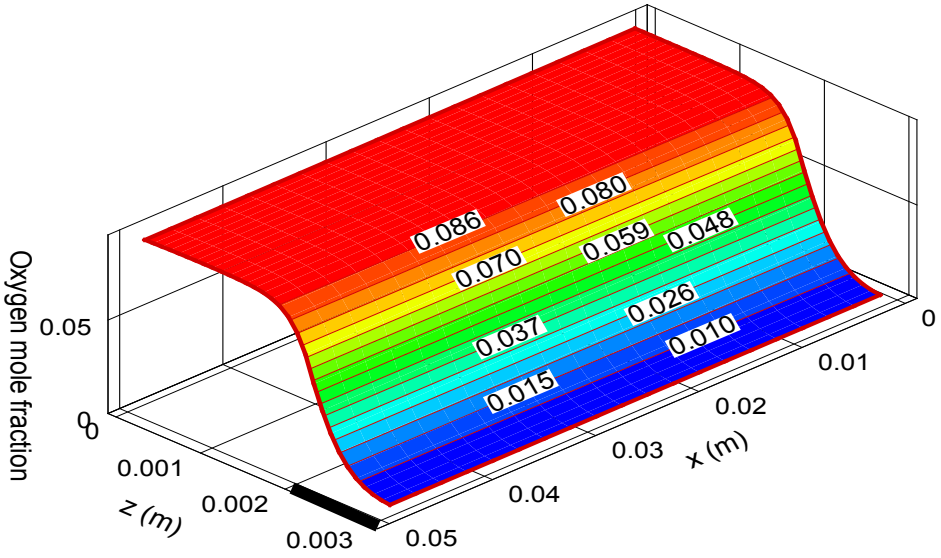

Fig. 5.16 Oxygen concentration distribution after diffusion through the membrane film in the catalyst layer. V=0.25V. Anode humidification Temp. = 70°C; Cathode humidification Temp. = 70°C; Hydrogen flow rate = 500sccm; Air flow rate = 2000sccm; Fuel cell pressure = 1atm.

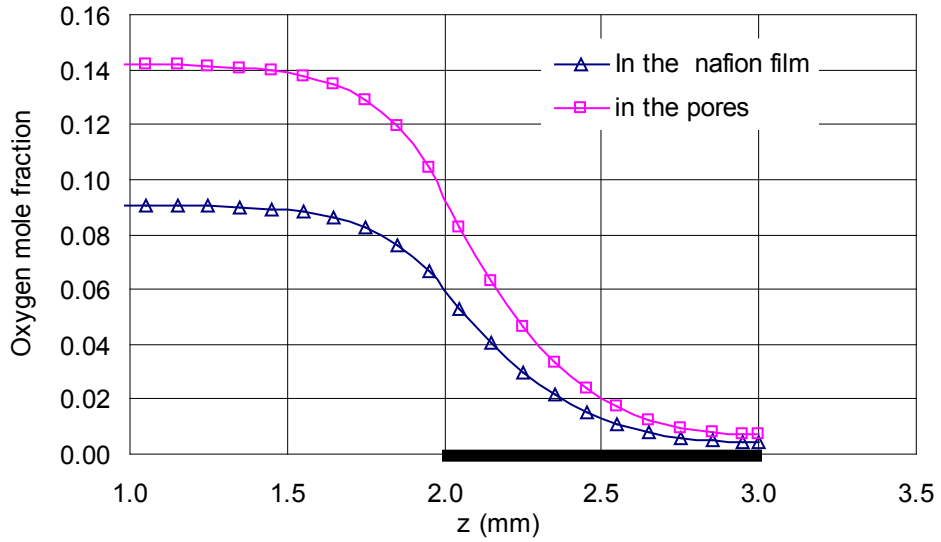

Fig. 5.17 Comparison of oxygen concentration distribution before and after diffusion through the membrane film in the catalyst layer. V=0.25V. Anode humidification Temp. = 70°C; Cathode humidification Temp. = 70°C; Hydrogen flow rate = 500sccm; Air flow rate = 2000sccm; Fuel cell pressure = 1atm. (x/L=0.5)

Overpotential distribution

The overpotential distributions along the cross-channel direction with cell voltage of 0.6V and 0.26V are shown in Fig. 5.18 and 5.19 respectively. The overpotential under the shoulder is always higher than that under the channel, because of the lateral electric resistance and the different through-plane electric resistance of the gas diffusion layer under the channel and under the shoulder.

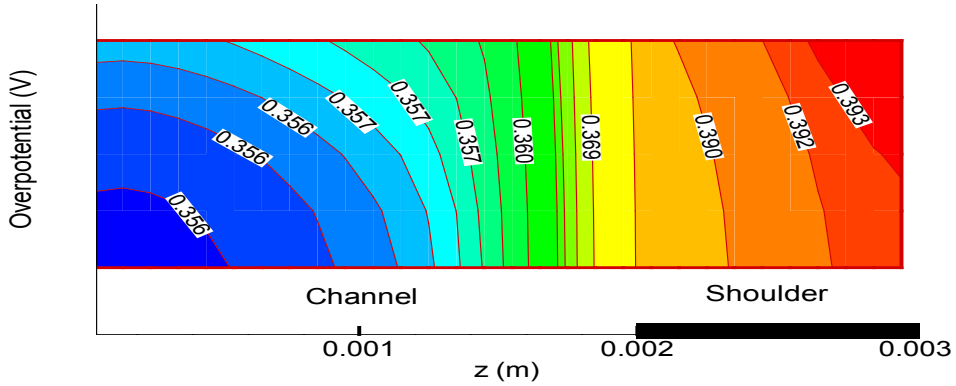

Fig. 5.18 Overpotential distribution in the catalyst layer. V=0.6V. Anode humidification Temp. = 70°C; Cathode humidification Temp. = 70°C; Hydrogen flow rate = 500sccm; Air flow rate = 2000sccm; Fuel cell pressure = 1atm.

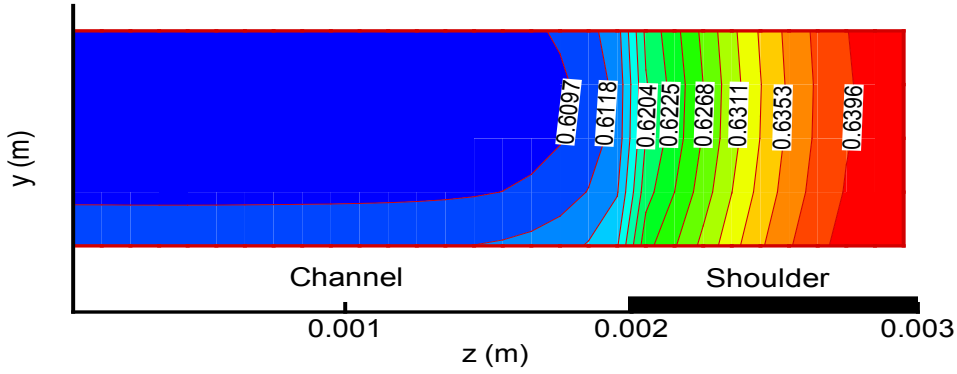

Fig. 5.19 Overpotential distribution in the catalyst layer. V=0.26V. Anode humidification Temp. = 70°C; Cathode humidification Temp. = 70°C; Hydrogen flow rate = 500sccm; Air flow rate = 2000sccm; Fuel cell pressure = 1atm.

Membrane phase potential distribution

Fig. 5.20 and 5.21 show the membrane phase potential in the catalyst layer and the membrane across the channel direction. The membrane phase current flows from the membrane side and consume in the catalyst layer, therefore the membrane phase potential decreases from the membrane heading to the catalyst layer.

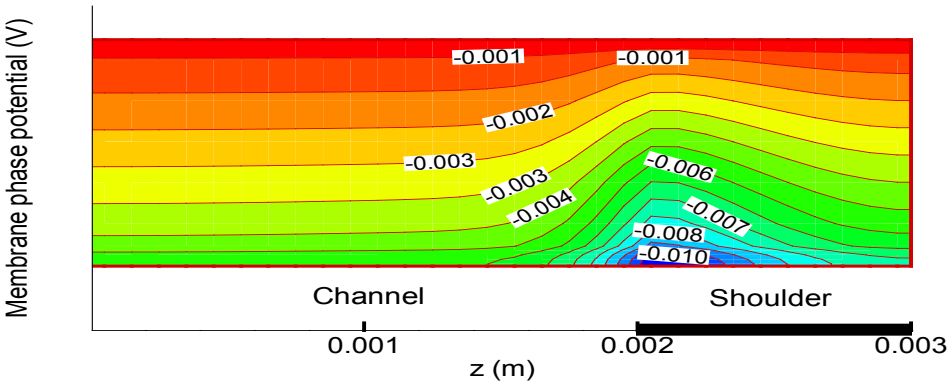

Fig. 5.20 Membrane phase potential distribution. V=0.6V. Anode humidification Temp. = 70°C; Cathode humidification Temp. = 70°C; Hydrogen flow rate = 500sccm; Air flow rate = 2000sccm; Fuel cell pressure = 1atm.

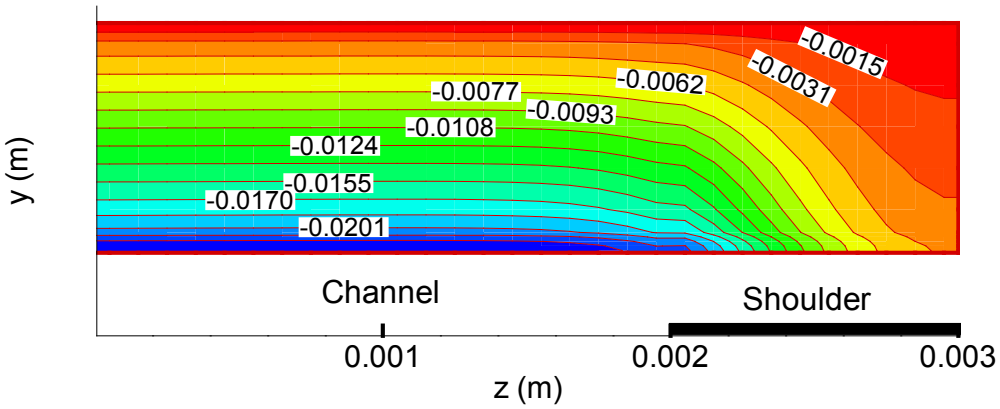

Fig. 5.21 Membrane phase potential distribution. V=0.25V. Anode humidification Temp. = 70°C; Cathode humidification Temp. = 70°C; Hydrogen flow rate = 500sccm; Air flow rate = 2000sccm; Fuel cell pressure = 1atm.

Solid phase potential distribution

The solid phase potential in the gas diffusion layer and the catalyst layer under the cell voltage of 0.6V and 0.26V has been shown in Fig. 5.22 and 5.23. The electrons flow from the collector plate connecting to the gas diffusion layer through the shoulder. In the catalyst layer electrons are consumed. Therefore the solid phase potential at the edge of the shoulder is lowest. With the flowing of electrons towards the catalyst layer, the potential increases.

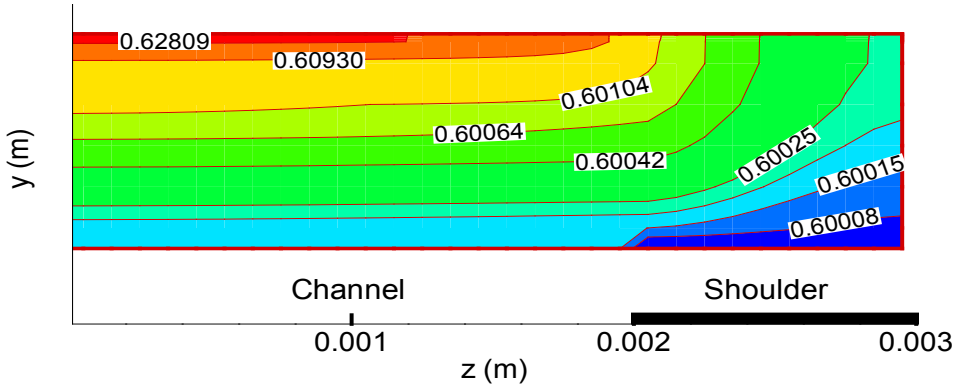

Fig. 5.22 Solid phase potential distribution. V=0.6V. Anode humidification Temp. = 70°C; Cathode humidification Temp. = 70°C; Hydrogen flow rate = 500sccm; Air flow rate = 2000sccm; Fuel cell pressure = 1atm.

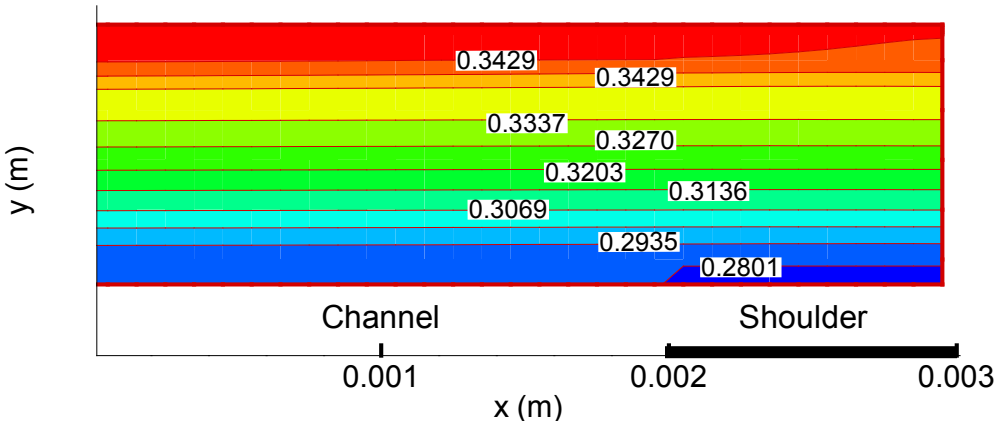

Fig. 5.23 Solid phase potential distribution. V=0.25V. Anode humidification Temp. = 70°C; Cathode humidification Temp. = 70°C; Hydrogen flow rate = 500sccm; Air flow rate = 2000sccm; Fuel cell pressure = 1atm.

5.3.2 Modeling results with constant through-plane electric conductivity

To test the effect of the lateral resistance on the current density distribution across the channel direction, the simulation of the experimental operation is also calculated by the mathematical model without considering the difference of the through-plane electric conductivity under the channel and under the shoulder.

Current density distribution

The current density distribution in the catalyst layer at the cell voltage of 0.6V is shown in Fig. 5.24. Although the lateral resistance is considered, the current density under the channel is still higher than that under the shoulder, which indicates that the overpotential difference caused by the lateral resistance is not big enough to overpass the impact of the oxygen concentration on the current distribution.

Oxygen Concentration distribution

The oxygen concentration in the pores and after the diffusion through the membrane film is shown in Fig. 5.25 and 5.26. From the comparison of the oxygen concentration in the pores and in the membrane film, which is shown in Fig. 5.27, it is observed that the oxygen concentration becomes more uniform.

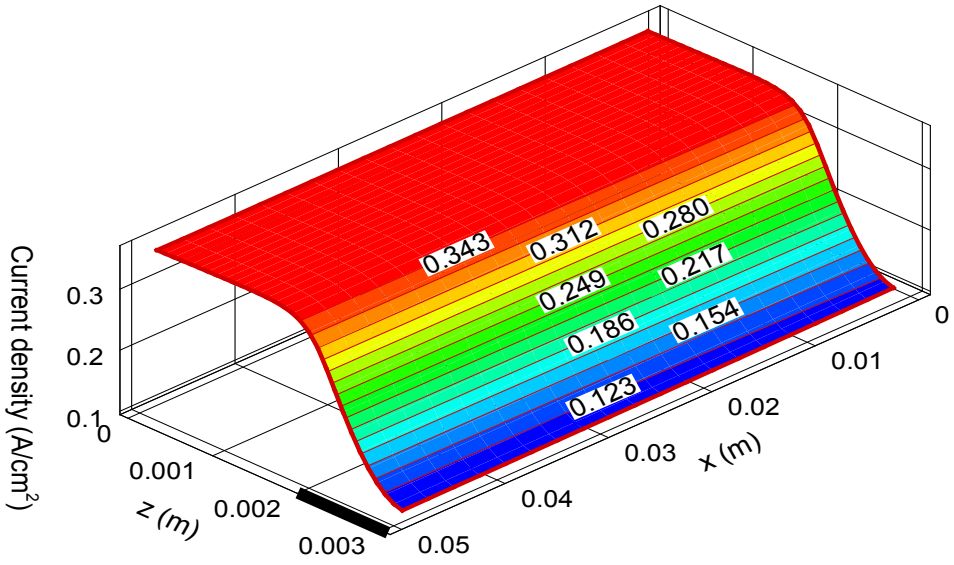

Fig. 5.24 Current density distribution in the catalyst layer. V=0.6V. Anode humidification Temp. = 70°C; Cathode humidification Temp. = 70°C; Hydrogen flow rate = 500sccm; Air flow rate = 2000sccm; Fuel cell pressure = 1atm.

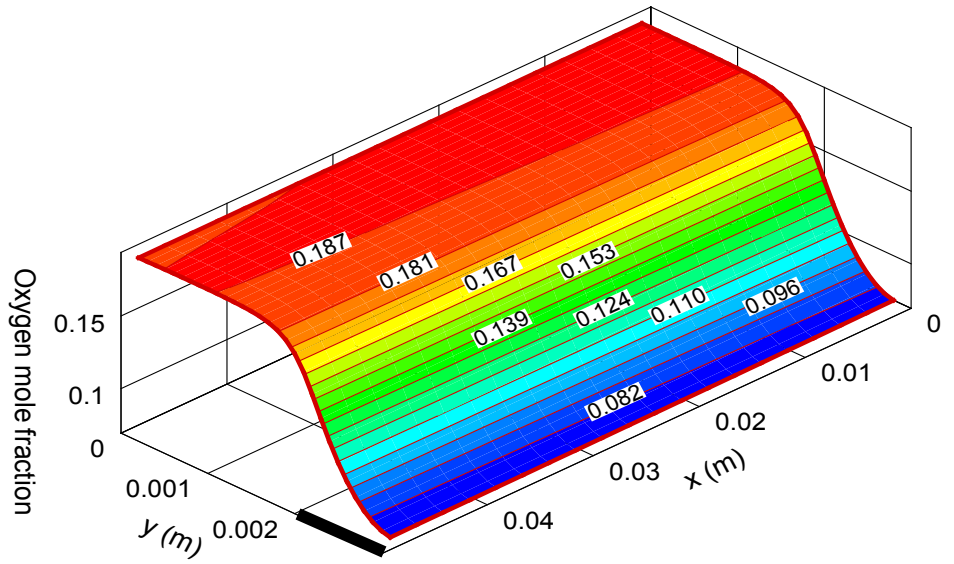

Fig. 5.25 Oxygen concentration distribution in the pores in the catalyst layer. V=0.6V. Anode humidification Temp. = 70°C; Cathode humidification Temp. = 70°C; Hydrogen flow rate = 500sccm; Air flow rate = 2000sccm; Fuel cell pressure = 1atm.

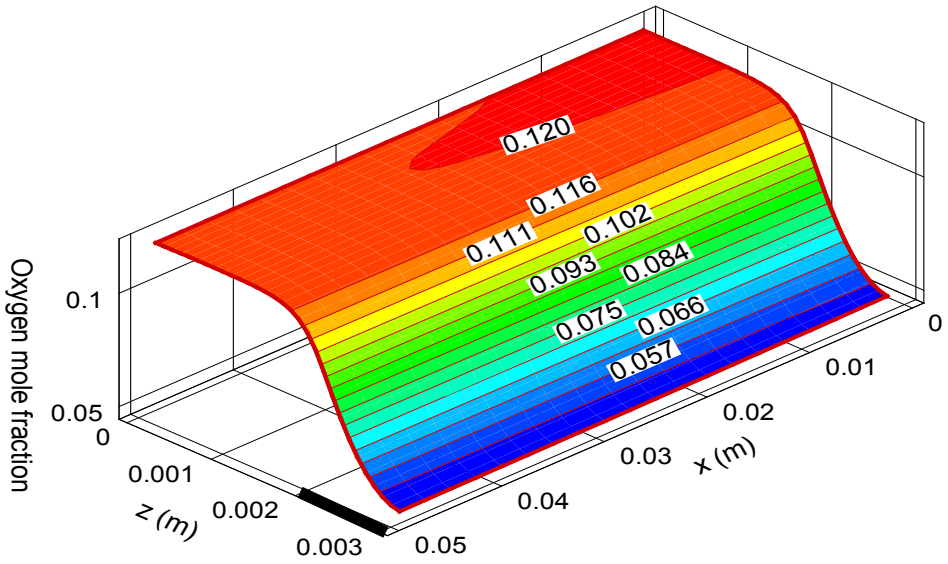

Fig. 5.26 Oxygen concentration distribution after diffusion through the membrane film in the catalyst layer. V=0.6V. Anode humidification Temp. = 70°C; Cathode humidification Temp. = 70°C; Hydrogen flow rate = 500sccm; Air flow rate = 2000sccm; Fuel cell pressure = 1atm.

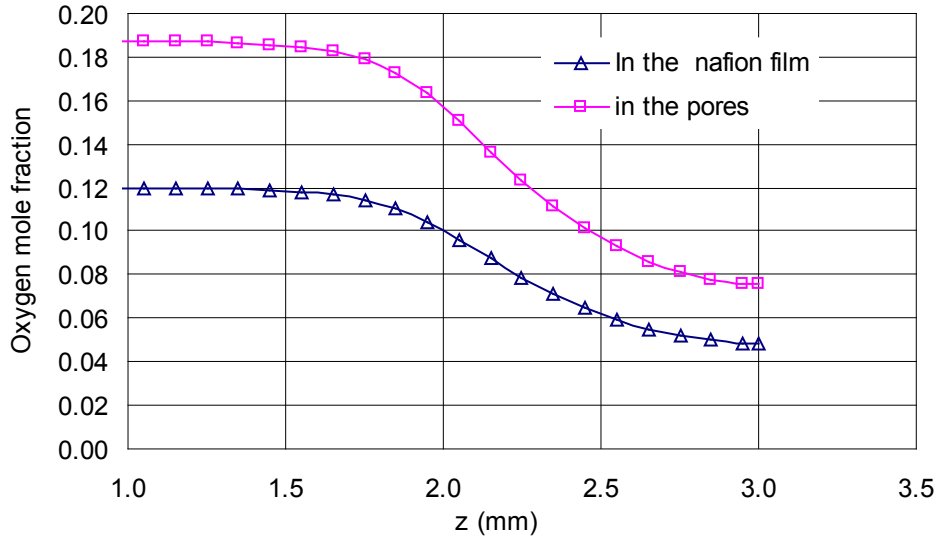

Fig. 5.27 Comparison of oxygen concentration distribution before and after diffusion through the membrane film in the catalyst layer. V=0.6V. Anode humidification Temp. = 70°C; Cathode humidification Temp. = 70°C; Hydrogen flow rate = 500sccm; Air flow rate = 2000sccm; Fuel cell pressure = 1atm. (x/L=0.5)

Overpotential distribution

The overpotential distribution in the catalyst layer is shown in Fig. 5.28. The difference of the overpotential under the channel and under the shoulder is smaller than the difference calculated when considering the through-plane electric resistance under the channel and under the shoulder. Therefore the lateral resistance itself can not cause the current density under the shoulder to be higher than that under the channel.

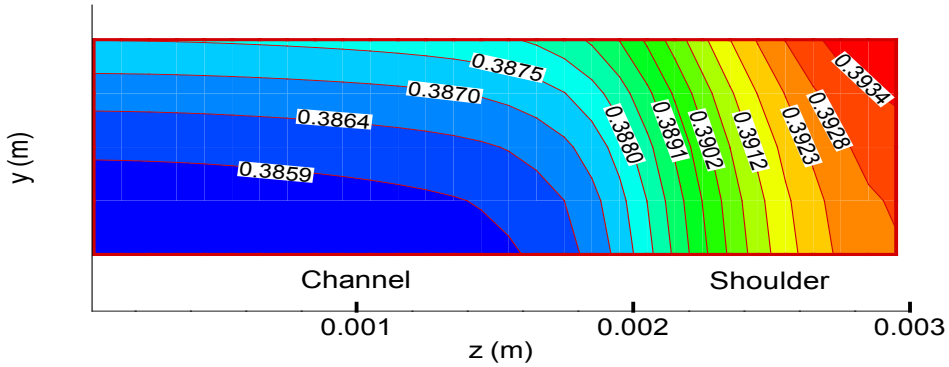

Fig. 5.28 Overpotential distribution after diffusion through the membrane film in the catalyst layer. V=0.5V. Anode humidification Temp. = 70°C; Cathode humidification Temp. = 70°C; Hydrogen flow rate = 500sccm; Air flow rate = 2000sccm; Fuel cell pressure = 1atm.

CHAPTER 6

CONCLUSIONS AND FUTURE RESEARCH

6.1 Conclusions

In this work, experimental and modeling studies on the effect of mass transport and GDL electric resistance on current density distribution of a PEM fuel cell have been carried out.

From the literature survey, it is found that there is limited experimental data on the current distribution along the across-channel direction of a PEM fuel cell. In addition, a few modeling studies on current distribution along the across-channel direction provided conflicting modeling results. Hence experiments have been conducted to measure the current density under the channel and under the shoulder. Moreover the effects of the lateral electric resistance and through-plane electric resistance of the gas diffusion layer on the current distribution have been studied experimentally. The following conclusion can be obtained:

- At the low load operation, the current density under the channel is lower than that under the shoulder. At the high load operation, the current density under the channel is higher that under the shoulder.
- The overpotential difference between under the channel and under the shoulder caused by the lateral resistance of the gas diffusion layer is not big enough to make the current density under the shoulder to be higher than that under the channel.

- The pressure difference of the gas diffusion layer under the channel and under the shoulder causes a significant difference of the through-plane electric resistance of the gas diffusion layer under the channel and under the shoulder. The low through-plane electric resistance difference will cause the higher current density under the shoulder.

A three-dimensional model of PEM fuel cells has been developed to study the effect of mass transport and GDL electric resistance on the current distribution in PEM fuel cells. The model is programmed using FORTRAN. Patankar's Simpler Method has been used to solve the governing equations.

In addition, a new method combing the thin-film model and the homogeneous model has been proposed and developed to model the cathode catalyst layer. The model is validated by the experimental data. The modeling results show that the homogeneous catalyst model considering the Nafion films around the catalyst is very close to the real catalyst layer. Hence this model can provide better simulations to the operations of PEM fuel cells.

6.2 Future Research

The experimental method to measure the current density under the channel and shoulder is validated by the experimental results, which is testified to be an effective method to measure the current distribution across the channel and the shoulder direction. In this work only one average current density is measured for the channel and the shoulder respectively. In the future, the same experimental method can be used to measure a series of current densities across the channel and the shoulder direction by making each division of the electrode less narrow. Then a more detailed current

distribution across the channel and the shoulder direction will be found. The experimental results will help people better understand the mechanism of operation of PEM fuel cells and will direct the optimization of PEM fuel cells.

The new mathematical model developed in this work shows a good simulation performance. Only the gas phase is considered in the model. In a real PEM fuel cell, water produced by the chemical reaction and carried with the humidified reactant gases is exist in both gas and liquid form. The existence of the liquid water can greatly affect the fuel cell performance, in the future. Therefore the current model is suggested to be improved by considering two-phase phenomenon, which will better simulate the effect of the water management on the fuel cell performance.

REFERENCES

Acres, G. J. K., Recent Advances in Fuel Cell Technology and Its Applications, J. Power Sources, **100**, 60, (2001)

Amphlett, J. C., Baumert, R. M., Mann, R. F., Peppley, B. A., and Roberge, P. R., Performance Modeling of the Ballard Mark IV Solid Polymer Electrolyte Fuel Cell, J. Electrochem. Soc., **142**, 1, (1995)

Bernardi, D. M., Water-Balance Calculations for Solid-Polymer-Electrolyte Fuel Cells, J. Electrochemical Society, **137**, 3344, (1990)

Bernardi, D. M. and Verbrugge, M. W., Mathematical Model of a Gas Diffusion Electrode Bonded to a Polymer Electrolyte, AIChE Journal, **37**, 1151, (1991)

Bernardi, D. M. and Verbrugge, M. W., A Mathematical Model of the Solid-Polymer-Electrolyte Fuel Cell, J. Electrochem. Soc., **139**, 2477, (1992)

Berning, T., Lu, D. M. and Djilali, N., Three-dimensional Computational Analysis of Transport Phenomena in a PEM Fuel Cell, J. Power Sources, **106**, 284, (2002)

Birgersson, E. and Vynnycky, M., A Quantitative Study of the Effect of Flow-Distributor Geometry in the Cathode of a PEM Fuel Cell, J. Power Sources, **153**, 76, (2006)

Brett, D., Atkins, S., Brandon, N., Vesovic, V., Vasileiadis, N. and Kucernak, A., Measurement of the Current Distribution Along a Single Flow Channel of a Solid Polymer Fuel Cell, Electrochemistry Communication, **3**, 628 (2001)

Broka, K. and Ekdunge, P., Modeling the PEM Fuel Cell Cathode, J. Applied Electrochemistry, **27**, 281, (1997)

Bultel, Y., Ozil, P. and Durand, R., Modified Thin Film and Agglomerate Models for Active Layers of P. E. Fuel Cells, *Electrochimica Acta*, **43**, 1077, (1998)

Büchi, F. N., Geiger, A. B. and Neto, R. P., Dependence of Current Distribution on Water Management in PEFC of Technical Size, J. Power Sources, **145**, 62, (2005)

Cleghorn, S.J., Derouin, C. R., Wilson, M.S. and Gotterfeld, S., A Printed Circuit Board Approach to Measuring Current Distribution in a Fuel Cell, J. Applied Electrochemistry, **28**, 663, (1998)

Dutta, S., Shimpalee, S. and Van Zee, J.W., Three-dimensional Numerical Simulation of Straight Channel PEM Fuel Cells, J. Applied Electrochemistry, **30**, 135, (2000)

Eikerling, M., Kornyshev, A. A., and Stimming, U., Electrophysical Properties of Electrolyte Membranes: a Random Network Model, J. Physical Chemistry B, **101**, 10807, (1997)

Eikerling, M. and Kornyshev, A. A., Modeling the Performance of the Cathode Catalyst Layer of Polymer Electrolyte Fuel Cells, J. Electroanalytical Chemistry, **453**, 89, (1998)

Freunberger, S. A., Reum, M., Evertz, J., Wokaun, A. and Büchia, F. N., Measuring the Current Distribution in PEFCs with Sub-Millimeter Resolution, I. Methodology, J. Electrochem. Society, **153**, A2158, (2006)

Fuller, T. F. and Newman, J. Water and Thermal Management in Solid-Polymer-Electrolyte Fuel Cells, J. Electrochem. Soc., **140**, 1218, (1993)

Ghosh, P. C., Wüster, T., Dohle, H., Kimiaie, N., Mergel, J. and Stolten, D., Analysis of Single PEM Fuel Cell Performances Based on Current Density Distribution Measurement, J. of Fuel Cell Science and Technology, **3**, 351, (2006)

Giner, J. and Hunter, C., The Mechanism of Operation of the Teflon-Bonded Gas Diffusion Electrode: A Mathematical Model, J. Electrochem. Soc., **147**, 1124, (1969)

Gloaguen, F. and Durand, R., Simulations of PEFC Cathodes: an Effective Factor Approach, J. Applied Electrochemistry, **27**, 1029, (1997)

Gurau, V., Barbir, F. and Liu, H., An Analytical Solution of a Half-Cell Model for PEM Fuel Cell, J. Electrochem. Soc., **147**, 2468, (2000)

Gurau, V., Liu, H. and Kakac, S., Two-Dimensional Model for Proton Exchange Membrane Fuel Cells, AICHE J., **44**, 2410, (1998)

Hakenjos, A., Muenter, H., Wittstadt, U. and Hebling, C., A PEM Fuel Cell for Combined Measurement of Current and Temperature Distribution, and flow Field Flooding, J. Power Sources, **131**, 213, (2004)

Hakenjos, A., Tüber, K., Schumacher, J. O. and Hebling, C., Characterising PEM fuel Cell Performance Using a Current Distribution Measurement in Comparison with a CFD Model, Fuel Cells, **4**, 185, (2004)

Hakenjos, A. and Hebling, C., Spatially Resolved Measurement of PEM Fuel Cells, J. Power Sources, **145**, 307, (2005)

Hogarth,W. H. J., Steiner, J., Benziger, J. B. and Hakenjos, A., Spatially-resolved Current and Impedance Analysis of a Stirred Tank Reactor and Serpentine Fuel Cell Flow-field at Low Relative Humidity, J. Power Sources, **164**, 464, (2007)

Hottinen, T., Noponen, M., Mennola, T., Himanen, O., Mikkola, M. and Lund, P., Effect of Ambient Conditions on Performance and Current Distribution of a Polymer Electrolyte Membrane Fuel Cell, J. Applied Electrochemistry, **33**, 265, (2003)

Jaouen F., Lindbergh, G. and Sundholm, G., Investigation of Mass-Transport Limitations in the Solid Polymer Fuel Cell Cathode, I. Mathematical Method, J. Electrochem. Soc., **149**, A437, (2002)

Ju., H. and Wang, C., Experimental Validation of a PEM Fuel Cell Model by Current Distribution Data, J. Electrochem. Soc., **151**, A1954, (2004)

Lin, G., He, W. and Nguyen, T. V., Modeling Liquid Water Effects in the Gas Diffusion and Catalyst layers of the Cathode of a PEM Fuel Cell, J. Electrochem. Soc., **151**, A1999, (2004)

Lin, G., and Nguyen, T. V., A Two-Dimensional Two-Phase Model of a PEM Fuel Cell, J. Electrochem. Soc., **153**, A372, (2006)

Liu Z., Mao, Wu, Z., Wang, B., L. and Schmidt, V. M., Current Density Distribution in PEFC, J. Power Sources, **141**, 205, (2005)

Liu, X., Tao, W., Li, Z. and He, Y., Three-dimensional Transport Model of PEM Fuel Cell with Straight Flow Channels, *J. Power Sources*, **158**, 25, (2006)

Madhsudana, R. and Rengaswamy, R. R., Dynamic Characteristics of Spherical Agglomerate for Study of Cathode Catalyst Layers in Proton Exchange Membrane Fuel Cells (PEMFC), J. Power Sources, **158**, 110, (2006)

Marr, C. and Li, X., Composition and Performance Modeling of Catalyst Layer in a Proton Exchange Membrane Fuel Cell, J. Power Sources, **77**, 17, (1999)

Mench, M.M., Wang, C.Y. and Ishikawa, M., In Situ Current Distribution Measurements in Polymer Electrolyte Fuel Cells, J. Electrochem. Soc., **150**, A1052, (2003)

Meng, H. and Wang, C. Y., Electron Transport in PEFCs, J. Electrochem. Soc., 151, A358, (2004)

Natarajan, D. and Nguyen, T. V., Effect of Electrode Configuration and Electronic Conductivity on Current Density Distribution Measurement in PEM Fuel Cells, J. Power Sources, **135**, 95, (2004)

Natarajan, D. and Nguyen, T. V., A Two-Dimensional, Two-Phase, Multicomponent, Transient Model for the Cathode of a Proton Exchange Membrane Fuel Cell Using Conventional Gas Distributors, J. Electrochem. Soc., **148**, A1324, (2001)

Natarajan, D. and Nguyen, T. V., Current Distribution in PEM Fuel Cells. Part 1: Oxygen and Fuel Flow Rate Effects, AICHE Journal, **51**, 2587, (2005)

Natarajan, D. and Nguyen, T. V., Current Distribution in PEM Fuel Cells. Part 2: Air Operation and Temperature Effect, AICHE Journal, **51**, 2599, (2005)

Nguyen, T. V. and White, R. E., A Water and Heat Management Model for Proton-Exchange-Membrane Fuel Cells, J. Electrochem. Soc., **40**, 2178, (1993)

Nguyen, P. T., Berning, T. and Djilali, N., Computational Model of a PEM Fuel Cell with Serpentine Gas Flow Channels, J. Power Sources, **130**, 149, (2004)

Noponen, M., Mennola, T., Mikkola, M., Hottinen, T. and Lund, P., Measurement of Current Distribution in a Free-breathing PEMFC, J. Power Sources, **106**, 304, (2002)

Noponen, M., Ihonen, J., Lundblad, A. and Lindbergh, G., Current Distribution Measurement in a PEFC with Net Flow Geometry, **34**, 255, (2004).

Patankar, S. V., Numerical heat transfer and fluid flow, Hemisphere, Washington, DC, (1980)

Prater, K., The Renaissance of the Solid Polymer Fuel Cell, J. Power Sources, **29**, 239, (1990)

Rajalakshmi, N., Raja, M. and Dhathathreyan, K. S., Evaluation of Current Distribution in a Proton Exchange Membrane Fuel Cell by Segmented Cell Approach, J. Power Sources, **112**, 331-336, (2002)

Shimpalee, S., Greenway, S., Spuckler, D. and Van Zee, J. W., Predicting Water and Current Distributions in a Commercial-size PEMFC, J. Power Sources, **135**, 79, (2004)

Siegel, N. P., Ellis, M. W., Nelson, D. J. and Von Spakovsky, M. R., Single Domain PEMFC Model Based on Agglomerate Catalyst Geometry, J. Power Sources, **115**, 81, (2003)

Sivertsen, B. R. and Djilali, N., CFD-based Modeling of Proton Exchange Membrane Fuel Cells, J. Power Sources, **141**, 65, (2005)

Springer, T. E., Zawodzinski, T. A. and Gottesfeld, S., Polymer Electrolyte Fuel Cell Model, J. Electrochem. Soc., **138**, 2334, (1991)

Springer, T. E., Wilson, M. S., and Gottesfeld, S., Modeling and Experimental Diagnostics in Polymer Electrolyte Fuel Cells, J. Electrochem. Soc., **140**, 3513, (1993)

Srinivasan, S. and Hurwitz, H. D., Theory of a Thin Film Model of Porous Gas-diffusion Electrodes, Electrochimica Acta, **12**, 495, (1967)

Stumper, J., Campbell, S.A., Wilkinson, D.P., Johnson, M. C. and Davis, M., In-situ Methods for the Determination of Current Distribution in PEM Fuel Cells, Electrochimica Acta, **43**, 3773, (1998)

Sun, W., Peppley, B. A. and Karan, K., An Improved Two-dimensional Agglomerate Cathode Model to Study the Influence of Catalyst Layer Structural Parameters, Electrochimica Acta, **50**, 3359, (2005)

Sun, H., Zhang, G., Guo, L. and Liu, H., A Novel Technique for Measuring Current Distributions in PEM Fuel Cells, J. Power Sources, **158**, 326, (2006)

Um, S., Wang, C.Y. and K. S. Chen, Computational Fluid Mechanics of Proton Exchange Membrane Fuel Cells, J. Electrochem. Soc., **147**, 4485, (2000)

Um, S. and Wang, C.Y., Three-dimensional Analysis of Transport and Electrochemical Reactions in Polymer Electrolyte Fuel Cells, J. Power Sources, **125**, 40, (2004)

Verbrugge, M.W. and Hill, R.F., Ion and Solvent Transport in Ion-Exchange Membranes - I. A Macrohomogeneous Mathematical Model, J. Electrochemical Society, **137**, 886, (1990a)

Verbrugge, M.W. and Hill, R.F., Ion and Solvent Transport in Ion-Exchange Membranes - II. A Radiotracer Study of the Sulfuric-Acid, Nafion-117 System, J. Electrochemical Society, **137**, 893, (1990b).

Verbrugge, M.W. and Hill, R.F., Analysis of Promising Perfluorosulfonic Acid Membranes for Fuel-Cell Electrolytes, J. Electrochemical Society, **137**, 3770, (1990c)

Wang, Z. H., Wang, C. Y. and Chen, K. S., Two-phase Flow and Transport in the Air Cathode of Proton Exchange Membrane Fuel Cells, J. Power Sources, **94**, 40, (2001).

Wang, Q., Eikerling, M., Song, D. and Liu, Z., Structure and Performance of Different Types of Agglomerates in Cathode Catalyst Layers of PEM Fuel Cells, J. Power Sources, **573**, 61, (2004).

Wang, Q., Song, D., Navessin, T., Holdcroft, S. and Liu, Z., A Mathematical Model and Optimization of the Cathode Catalyst Layer Structure in PEM Fuel Cells, Electrochimica Acta, **50**, 725, (2004).

Wieser, C., Helmbold, A. and Gulzow, E., A New Technique for Two-dimensional Current Distribution Measurements in Electrochemical Cells, J. Applied Electrochemistry, **30**, 803, (2000).

Will, F. G., J. Electrochem. Soc., **110**, 152 (1963A).

Will, F. G., J. Electrochem. Soc., **110**, 145 (1963B).

Wüster, T., Dohle, H., Kimiaie, Mergel, N., J. and Stolten, D., Analysis of Single PEM Fuel Cell Performances Based on Current Density Distribution Measurement, J. Fuel Cell Science and Technology, **3**, 351, (2006).

Yi, J. S. and Nguyen, T. V., An Along-the Channel Model for PEM Fuel Cell, J. Electrochem. Soc., **145**, 1149, (1998)

You, L. and Liu, H., A Parametric Study of the Cathode Catalyst Layer of PEM Fuel Cells Using a Pseudo-homogeneous Model, International Journal of Hydrogen Energy, **26**, 991, (2001)

You, L. and Liu, H., A Two-Phase Flow and Transport Model for the Cathode of PEM Fuel Cells, International Journal of Heat and Mass Transfer, **45**, 2277, (2002).

Zhou, T. and Liu, H., A General Three-Dimensional Model for Proton Exchange Membrane Fuel Cell, I. J. Trans. Phenomena, **3**, 177-198, (2001).

Zhou, T. and Liu, H., Effects of the Electrical Resistances of the GDL in a PEM Fuel Cell, J. Power Sources, 161, **444**, (2006).

APPENDIX

Table A1 Data of the Polarization Curves of the PEM Fuel Cell with Full Catalyst Loading. Anode humidification Temp. = 70°C; Cathode humidification Temp. = 70°C; Hydrogen flow rate = 500sccm; Air flow rate = 2000sccm.

1atm		1.68atm		2.36atm		3.72atm	
Current density (A/cm^2)	Voltage (V)	Current density (A/cm^2)	Voltage (V)	Current density (A/cm^2)	Voltage (V)	Current density (A/cm^2)	Voltage (V)
0. 003	0. 932	0. 003	0. 956	0. 003	0. 956	0. 003	0. 973
0. 003	0. 932	0. 003	0. 956	0. 003	0. 956	0. 003	0. 956
0. 003	0. 890	0. 009	0. 890	0. 009	0. 890	0. 015	0. 890
0. 019	0. 841	0. 024	0. 841	0. 028	0. 841	0. 060	0. 841
0. 043	0. 799	0. 048	0. 799	0. 079	0. 799	0. 092	0. 799
0. 084	0. 741	0. 083	0. 758	0. 119	0. 758	0. 168	0. 750
0. 132	0. 692	0. 147	0. 700	0. 208	0. 692	0. 243	0. 700
0. 177	0. 658	0. 211	0. 642	0. 302	0. 642	0. 330	0. 650
0. 248	0. 601	0. 282	0. 601	0. 352	0. 601	0. 405	0. 609
0. 307	0. 559	0. 346	0. 559	0. 430	0. 559	0. 509	0. 559
0. 381	0. 502	0. 430	0. 502	0. 513	0. 502	0. 573	0. 510
0. 464	0. 443	0. 509	0. 435	0. 604	0. 443	0. 649	0. 435
0. 534	0. 394	0. 577	0. 394	0. 658	0. 394	0. 732	0. 394
0. 579	0. 344	0. 638	0. 344	0. 717	0. 336	0. 766	0. 344
0. 609	0. 311	0. 683	0. 294	0. 772	0. 294	0. 832	0. 294
0. 688	0. 261	0. 747	0. 245	0. 815	0. 245	0. 866	0. 245

Table A2 Data of the Polarization Curves of the PEM Fuel Cell with Catalyst Loading under the shoulder. Anode humidification Temp. = 70°C; Cathode humidification Temp. = 70°C; Hydrogen flow rate = 500sccm; Air flow rate = 2000sccm.

1atm		1.68atm		2.36atm		3.72atm	
Current density (A/cm^2)	Voltage (V)	Current density (A/cm^2)	Voltage (V)	Current density (A/cm^2)	Voltage (V)	Current density (A/cm^2)	Voltage (V)
0. 009	0. 923	0. 009	0. 932	0. 009	0. 940	0. 003	0. 973
0. 009	0. 923	0. 009	0. 932	0. 009	0. 940	0. 003	0. 956
0. 009	0. 890	0. 009	0. 890	0. 009	0. 890	0. 015	0. 890
0. 027	0. 841	0. 027	0. 841	0. 040	0. 841	0. 060	0. 841
0. 051	0. 799	0. 058	0. 799	0. 085	0. 791	0. 092	0. 799
0. 116	0. 741	0. 143	0. 741	0. 143	0. 750	0. 168	0. 750
0. 161	0. 700	0. 250	0. 700	0. 205	0. 708	0. 243	0. 700
0. 237	0. 650	0. 295	0. 658	0. 308	0. 650	0. 330	0. 650
0. 308	0. 601	0. 357	0. 609	0. 397	0. 609	0. 405	0. 609
0. 354	0. 559	0. 473	0. 543	0. 504	0. 543	0. 509	0. 559
0. 415	0. 493	0. 531	0. 502	0. 563	0. 510	0. 573	0. 510
0. 473	0. 435	0. 576	0. 443	0. 634	0. 443	0. 649	0. 435
0. 531	0. 386	0. 638	0. 386	0. 665	0. 402	0. 732	0. 394
0. 565	0. 336	0. 652	0. 344	0. 696	0. 353	0. 766	0. 344
0. 586	0. 294	0. 696	0. 294	0. 759	0. 294	0. 832	0. 294
0. 607	0. 245	0. 696	0. 245	0. 813	0. 245	0. 866	0. 245

Table A3 Data of the Polarization Curves of the PEM Fuel Cell with Catalyst Loading under the channel. Anode humidification Temp. = 70°C; Cathode humidification Temp. = 70°C; Hydrogen flow rate = 500sccm; Air flow rate = 2000sccm.

1atm		1.68atm		2.36atm		3.72atm	
Current density (A/cm^2)	Voltage (V)	Current density (A/cm^2)	Voltage (V)	Current density (A/cm^2)	Voltage (V)	Current density (A/cm^2)	Voltage (V)
0. 004	0. 890	0. 004	0. 923	0. 004	0. 940	0. 004	0. 948
0. 004	0. 890	0. 004	0. 923	0. 004	0. 940	0. 004	0. 956
0. 004	0. 882	0. 004	0. 890	0. 013	0. 890	0. 004	0. 890
0. 004	0. 841	0. 022	0. 841	0. 029	0. 841	0. 036	0. 841
0. 029	0. 807	0. 058	0. 791	0. 065	0. 791	0. 071	0. 791
0. 058	0. 741	0. 087	0. 750	0. 118	0. 750	0. 118	0. 758
0. 103	0. 708	0. 132	0. 708	0. 170	0. 700	0. 170	0. 700
0. 154	0. 642	0. 199	0. 650	0. 221	0. 650	0. 243	0. 658
0. 230	0. 609	0. 268	0. 601	0. 297	0. 609	0. 342	0. 601
0. 295	0. 559	0. 386	0. 551	0. 408	0. 543	0. 424	0. 551
0. 371	0. 510	0. 467	0. 502	0. 478	0. 502	0. 504	0. 502
0. 496	0. 435	0. 578	0. 435	0. 571	0. 435	0. 607	0. 443
0. 565	0. 394	0. 629	0. 402	0. 658	0. 394	0. 734	0. 394
0. 658	0. 344	0. 728	0. 348	0. 741	0. 344	0. 830	0. 336
0. 705	0. 294	0. 839	0. 311	0. 837	0. 294	0. 882	0. 294
0. 732	0. 245	0. 866	0. 261	0. 929	0. 261	0. 987	0. 245

Table A4 Data of the Polarization Curves of the PEM Fuel Cell with Catalyst Loading under the channel without Silver Mesh. Anode humidification Temp. = 70°C; Cathode humidification Temp. = 70°C; Hydrogen flow rate = 500sccm; Air flow rate = 2000sccm.

1atm		1.68atm		2.36atm		3.72atm	
Current density (A/cm^2)	Voltage (V)	Current density (A/cm^2)	Voltage (V)	Current density (A/cm^2)	Voltage (V)	Current density (A/cm^2)	Voltage (V)
0. 004	0. 923	0. 004	0. 923	0. 004	0. 940	0. 004	0. 940
0. 004	0. 923	0. 004	0. 923	0. 004	0. 940	0. 004	0. 940
0. 004	0. 890	0. 004	0. 890	0. 013	0. 890	0. 013	0. 890
0. 022	0. 841	0. 022	0. 841	0. 029	0. 849	0. 029	0. 849
0. 036	0. 799	0. 036	0. 799	0. 058	0. 799	0. 065	0. 799
0. 065	0. 750	0. 103	0. 741	0. 118	0. 750	0. 109	0. 741
0. 134	0. 708	0. 156	0. 700	0. 185	0. 708	0. 183	0. 692
0. 192	0. 650	0. 237	0. 650	0. 259	0. 658	0. 243	0. 658
0. 275	0. 592	0. 304	0. 601	0. 393	0. 609	0. 357	0. 609
0. 348	0. 551	0. 371	0. 559	0. 460	0. 551	0. 438	0. 551
0. 438	0. 502	0. 475	0. 510	0. 580	0. 510	0. 549	0. 510
0. 542	0. 443	0. 580	0. 435	0. 667	0. 435	0. 690	0. 443
0. 600	0. 386	0. 719	0. 402	0. 770	0. 386	0. 757	0. 386
0. 690	0. 353	0. 786	0. 344	0. 866	0. 344	0. 830	0. 344
0. 770	0. 303	0. 844	0. 303	0. 911	0. 294	0. 866	0. 294
0. 866	0. 261	0. 929	0. 261	0. 942	0. 261	0. 942	0. 245

Table A5 Data of the Polarization Curves of the PEM Fuel Cell with Catalyst Loading under the channel with Silver Mesh. Anode humidification Temp. = 70°C; Cathode humidification Temp. = 70°C; Hydrogen flow rate = 500sccm; Air flow rate = 2000sccm.

1atm		1.68atm		2.36atm		3.72atm	
Current density (A/cm^2)	Voltage (V)	Current density (A/cm^2)	Voltage (V)	Current density (A/cm^2)	Voltage (V)	Current density (A/cm^2)	Voltage (V)
0.004	0.923	0.004	0.940	0.004	0.940	0.004	0.932
0.004	0.923	0.004	0.940	0.004	0.948	0.004	0.932
0.004	0.890	0.004	0.890	0.022	0.890	0.004	0.890
0.013	0.841	0.029	0.841	0.036	0.841	0.042	0.841
0.042	0.791	0.042	0.791	0.067	0.791	0.074	0.807
0.074	0.741	0.074	0.750	0.116	0.750	0.125	0.750
0.134	0.700	0.147	0.700	0.179	0.708	0.199	0.708
0.179	0.642	0.237	0.642	0.237	0.642	0.304	0.650
0.230	0.609	0.310	0.592	0.326	0.609	0.393	0.609
0.326	0.559	0.379	0.559	0.422	0.551	0.513	0.559
0.422	0.510	0.482	0.502	0.511	0.510	0.587	0.510
0.563	0.443	0.571	0.443	0.661	0.443	0.688	0.435
0.607	0.394	0.674	0.394	0.770	0.394	0.763	0.394
0.741	0.344	0.763	0.353	0.801	0.353	0.846	0.353
0.799	0.303	0.853	0.294	0.875	0.294	0.913	0.294
0.853	0.261	0.897	0.261	0.973	0.261	1.000	0.245